A Model for Turbulent Compressible Vortices

GURPREET SINGH BADWAL

A Thesis

In The Department

Of

Mechanical Engineering

Presented in Partial Fulfillment of the Requirements

for the Degree of Master of Applied Science (Mechanical Engineering)

at Concordia University

Montreal, Quebec, Canada

March 2014

Concordia University

School of Graduate Studies

This is to certify that the thesis prepared

By: GURPREET SINGH BADWAL

Entitled: A Model for Turbulent Compressible Vortices

and submitted in partial fulfillment of the requirements for the degree of

Master of Applied Science in Mechanical Engineering

Complies with regulations of the University and meets the accepted standards with respect to originality and quality.

Signed by the final examining committee:

Dr. M. Paraschivoiu	Chair
Dr. S. Samuel Li	Examiner
Dr. Ali Dolatabadi	Examiner
Dr. Georgios H. Vatistas	Supervisor

Approved By: Chair of Department or Graduate Program Director

Dean of Faculty

Date March 19th, 2014

Abstract

A Model for Turbulent Compressible Vortices

Gurpreet Singh Badwal

In this thesis the effects of turbulence are introduced by combining the past turbulent tangential velocity model with the preceding work on the laminar compressible vortices. The radial and axial velocity components are derived from the tangential and mass conservation equations. The temperature is then found numerically from the energy equation. Upon code verification several characteristics of the problem have been examined in detail.

The mysterious temperature separation is known since 1933 from the work of first Ranque and then Hilsch. Although several possibilities for its origin have been suggested no comprehensive theory for its causality has yet reported. The present novel approach is used to show conclusively that the cause of the thermal effect is the product of competition between the heating up of the gas because of friction and cooling due to material element expansion as it moves towards the region of decreasing pressure.

As originally inferred empirically, it is now shown theoretically that stream wise vortices within supersonic flow fields and high Rossby number atmospheric vortices such as tornadoes and waterspouts, display the classical heating/cooling effect. The new information is used to elaborate on several, yet inexplicable instrument recordings related to these natural phenomena. Finally the new results are used to justify some odd

physiological encounters made by several witnesses, trapped inside overpassing tornado's funnels, and lived to tell their unusual experiences.

The new basic methodology and findings can now be used to improve the design of vortex tubes.

Keywords: Vortex model, compressible vortices, turbulent vortices, temperature separation.

Acknowledgments

Foremost I would like to express my sincere thanks to my life supervisor Dr. Georgios H. Vatistas who has supported me throughout my thesis with his continuous financial support, motivation, immense knowledge and for spending time to read this thesis and providing me with useful suggestions. This thesis would not have been possible without his patience and advice. I shall always be very thankful to him for giving me the opportunity to be a part of his research team and also for his friendly character.

I would like to express my special thanks to my parents and elder sister for their continuous encouragement, wishes, patience and all of the sacrifices that they have made on my behalf. I owe my deepest gratitude to my uncle "S.Satnam Singh and S.Udham Singh" for their prayers and well wishes towards me. Last but not least, I would like to acknowledge the appreciation and love that I received from my in laws family and beloved wife "Parminder Kaur Badwal".

To all of them and especially to my parents I dedicate this thesis

Father: S. Shiv Charan Singh

Mother: Mohinder Kaur

Table of Contents

List of Figures viii

List of Tables xi

Nomenclature xii

1 Introduction 1

2 Previous work and thesis objectives 5

2.1 Previous work 5

2.2 Thesis Objectives 8

3 The Governing Flow Equations 10

3.1 Laminar Compressible Vortex Flow 10

3.2 Turbulent Compressible Vortex Flow 18

3.3 The Boundary Conditions 21

4 Numerical Solution 23

4.1 Numerical Method Applied on Energy Equation under Laminar Flow assumption 23

4.2 Numerical Method Applied on Energy Equation under Turbulent Flow assumption 26

5 Implementation of the Matlab Code 28

5.1 Verification of Matlab Code 28

6 Results for Laminar Compressible Vortex Flow 31

6.1 Calculation of Density and Pressure 31

6.2 Effect of Prandtl Number 31

6.3 Effect of Mach number on Temperature, Density and Pressure 33

6.4 Second Law of Thermodynamics applied to Laminar Compressible Vortex Flow 36

6.5 Explanation of Decrease in Temperature towards Centre of Vortex 38

7 Results for Turbulent Compressible Vortex Flow 42

7.1 Verification of the numerical procedure 42

7.2 Results and discussion of mechanically produced vortices 48

8 The Ranque-Hilsch effect in Atmospheric Vortices 59

9 Conclusions 64

10 Future Work 66

References 67

Appendix A 71

Appendix B 77

List of Figures

Figure 3.1 Definition of the coordinate system. 11

Figure 3.2 Dimensionless tangential velocity profiles for laminar and turbulent vortices. 20

Figure 3.3 The radial velocity distribution for laminar and turbulent vortices..... 20

Figure 5.1 Maximum absolute relative percentage difference between the numerical and exact solution of the energy equation under laminar flow condition with M_0=0.8,Pr=2/3 and $\xi_\infty = 200$ 30

Figure 6.1 Variation of dimensionless pressure vs. vortex Mach number for a laminar vortex for Pr=2/3, number of nodes =20,000, $\xi_\infty = 200$. (Note that p/p_∞ is equivalent to $\Pi\gamma M_0^2$)..... 34

Figure 6.2 Variation of dimensionless temperature vs. vortex Mach number for a laminar vortex with Pr =2/3, ξ_∞ = 200, and number of nodes = 20,000. 35

Figure 6.3 Variation of Density vs. vortex Mach number for a laminar vortex with Pr =2/3, ξ_∞ = 200 and number of nodes = 20,000. 36

Figure 6.4 Change in Entropy with vortex Mach number for a laminar vortex with Pr =2/3, ξ_∞ = 200, and number of nodes = 20,000. 38

Figure 6.5 Net effect of heating and cooling of fluid element due to viscous dissipation and fluid element expansion respectively in a laminar vortex for M_0=0.4, with Pr =2/3, ξ_∞ = 200, and number of nodes = 20,000..... 40

Figure 7.1 Residual of solution of energy equation under turbulent compressible vortex flow condition with Pr=2/3, M_0= 0.8, a = 0.7, ξ_∞ = 200 and number of nodes=20,000... 43

Figure 7.2 Variation of temperature at vortex center vs. ξ_∞ with parameters M_0=0.8, Pr=2/3, number of nodes=20,000 and a=0.7..... 44

Figure 7.3 Validation of the calculated pressure profiles from Eq.6.1.2, and using the experimental data of Pivirotto (1966). These were performed in a gaseous-vortex reactor (cold), for advanced space propulsion. The comparisons with two datasets (M_0 = 0.51 and 0.98) show a fair agreement between the two. $\xi_\infty = 200$. 47

Figure 7.4 Variation of temperature vs. the radius for a = 0.7, Pr =2/3, $\xi_\infty = 200$, M_0 = 0.4 and number of nodes=20,000..... 48

Figure 7.5 Net effect of heating and cooling of fluid element due to viscous dissipation and expansion respectively for a=0.7, Pr=2/3, $\xi_\infty = 200$, $M_0 = 0.4$ and number of nodes=20,000. 50

Figure 7.6 Dimensionless temperature vs. vortex Mach number for turbulent vortex for a=0.7, Pr=2/3, $\xi_\infty = 200$ and number of nodes=20,000. 52

Figure 7.7 Dimensionless temperature variation with vortex Mach number for turbulent vortex for Pr=2/3, $\xi_\infty = 200$ and number of nodes=20,000. 53

Figure 7.8 Dimensionless pressure variation with vortex Mach number for turbulent vortex for Pr=2/3, $\xi_\infty = 200$ and number of nodes=20,000. 54

Figure 7.9 Dimensionless density changes vs. vortex Mach number for turbulent vortex for Pr=2/3, $\xi_\infty = 200$ and number of nodes=20,000. 55

Figure 7.10 Change in Entropy value with vortex Mach number for turbulent vortex for Pr=2/3, a=0.7, $\xi_\infty = 200$ and number of nodes=20,000. 56

Figure 7.11 Comparison of Change in Entropy of laminar and turbulent compressible vortex for Pr=2/3, $\xi_\infty = 200$ and number of nodes=20,000. 57

Figure 7.12 Effect of scaling constant (a) on temperature profile of turbulent vortex flow for Pr=2/3, $\xi_\infty = 200$, M_0 =0.4 and number of nodes=20,000..... 58

Figure 8.1 Temperature distribution in radial direction in degree Celsius for M_0 =0.63. 60

Figure 8.2 Density changes in $\left(Kg/m^3\right)$ in the radial direction for M_0=0.63..... 61

Figure 8.3 The temperature anomaly in mature waterspouts where $\Delta T = T - T_\infty$. (From: Golden (1974)). 63

List of Tables

Table 5-1 Comparison of exact solution of energy equation under laminar flow condition with numerical solution for Pr=2/3, ξ_∞ =200 and number of nodes=20,000. 29

Table 6-1 Comparison between solution of energy equation under laminar flow condition for values of Pr =2/3 and 0.707 for M_0 = 0.8, ξ_∞ = 200 and number of nodes = 20,000.. 32

Table 6-2 Comparison between solution of energy equation under laminar flow for Pr =2/3 and 0.716, for M_0 = 0.8, ξ_∞ = 200 and number of nodes = 20,000..... 33

Table 7-1 Comparison between solution of energy equation under turbulent flow condition for values of Pr =2/3 and 0.707 with M_0 =0.8, $\xi_\infty = 200$ and number of nodes=20,000. 45

Table 7-2 Comparison between solution of energy equation under turbulent flow condition for values of Pr=2/3 and 0.716 with M_0 =0.8, $\xi_\infty = 200$ and number of nodes=20000. 46

Nomenclature

c_p	Heat capacity at constant pressure	KJ / Kg K
c_v	Heat capacity at constant volume	KJ / Kg K
r, θ, z	Radial, azimuthal and axial coordinates	m
r_c	Core radius	m
T	Static temperature	K
q	Total velocity vector	m/s
V_r, V_θ, V_z	Radial, tangential and axial velocity components	m/s
$V_{\theta max}$	Maximum tangential velocity at the core	m/s
s	Specific entropy	KJ / Kg K
k	Thermal conductivity	W / m K
R	Gas constant	KJ / Kg K
p	Static pressure	N/m^2
u	Dimensionless radial velocity component	$V_r/V_{\theta max}$
w	Dimensionless axial velocity component	$V_z/V_{\theta max}, \zeta h$
V	Normalized tangential velocity component	$V_\theta/V_{\theta max}$

Re	Vortex Reynolds number	$\rho_\infty V_{\theta max} r_c / \mu$
U	Normalized radial velocity component	βReu
H	Normalized axial velocity component	βReh
Pr	Prandtl number	$\mu c_p / k$
M_0	Vortex Mach number	$V_{\theta max} / \sqrt{\gamma R T_\infty}$
m	Constant for turbulent flow	$\frac{a+1}{4}$
a	Scaling constant	
o	Order of magnitude	
X_r, X_θ, X_z	Body forces in (r, θ, z) directions	
f	$\xi^2 \left\{ \frac{d}{d\xi} \left(\frac{V}{\xi} \right) \right\}^2$	

Greek Letters

μ	Dynamic viscosity	Kg/ms
ρ	Density	Kg/m^3
γ	Specific heat ratio	c_p / c_v
ξ	Dimensionless coordinate	r / r_c

ζ	Dimensionless coordinate	z / r_c
Θ	Dimensionless static temperature	T/T_∞
β	Dimensionless density	ρ / ρ_∞
ΔS	Dimensionless entropy change	$\frac{s - s_\infty}{c_p}$
Π	Dimensionless static pressure	$p/\rho_\infty V_{\theta max}^2$
Φ	Energy dissipation function (because of viscosity)	

Operators used

∂	Partial derivative	
$\frac{D}{Dt}$	Material derivative	$\frac{\partial}{\partial t} + V_r \frac{\partial}{\partial r} + \frac{V_\theta}{r} \frac{\partial}{\partial \theta} + V_z \frac{\partial}{\partial z}$
∇^2		$\frac{\partial^2}{\partial r^2} + \frac{1}{r} \frac{\partial}{\partial r} + \frac{1}{r^2} \frac{\partial^2}{\partial \theta^2} + \frac{\partial^2}{\partial z^2}$

Subscripts

∞	Infinity
c	Vortex core
max	Velocity at the core
o	Properties on the vortex core

1 Introduction

Real fluid motion cannot be comprehended without the appearance of vortices. These emerge in every scale; from the smallest that is found in super-cooled liquids to even galaxies. Therefore, these can be seen in both the natural world and in engineering. Naturally generated vortices are the, dust devils, tornadoes, waterspouts, fire whirls, hurricanes, polar, oceanic, volcanic, or yet galactic vortices. In technology, vortices can be an undesirable consequence of fluid motion that engineers try to weaken if not erase. These include wingtip vortices in airplanes, ship and aero-vehicle propellers under full thrust. In other applications such as the vortex separators, vortex combustors and incinerators, Ranque-Hilsch tubes, and vortex heat exchangers, vortex separator, the vortex tube, vortex steam traps, various components of turbo-machinery, plasma arcs swirl action is crucial for the proper operation of the devise and the designer is aiming to produce it most efficiently.

Wingtip vortices emerge due to pressure differential below and above the wing surfaces. These are responsible for the induced drag, which reduces the wing's lift efficiency, the aircraft's maneuverability, and produce losses. Also they are responsible for generating vibration and noise.

In addition, the general concept of vortex flow can be by analogy of benefit to plasma physics, electromagnetism, and optics. All the previous mentioned reasons have made their study attractive to researchers in various disciplines for many years.

A free and forced vortex is characterized based on vorticity. In a forced vortex, the curl of velocity vector field is non-zero whereas it is equal to zero for free vortex. The core radius (r_c) is the radius where the tangential velocity attains a maximum, and the core is designated as the sector where $0 \le r \le r_c$. Intense or strong is the vortex where the magnitude of tangential velocity is much larger than both the radial and axial. In concentrated vortices most of the vorticity exists inside the core.

Helmholtz (1858) and Rankine (1858) initiated the scientific study of vortices. Their contributions opened the doors for research in the new area of vortex dynamics. Since then a large amount of information has been amassed that has led into their better understanding.

For the incompressible steady state kind classical vortex mathematical formulations are due to Rankine (1858), Burgers (1948), Sullivan (1959), and Scully (1975). Rankine's (1858) model is the simplest all of them. It assumes no radial and axial velocities and the tangential component is only a function of the radius. Inside the core, the tangential velocity varies proportionally with the radius (forced-vortex) while outside it is inversely proportional to the radius (free- or potential-vortex). There is no discontinuity in the velocity profile but it has a sharp peak at the point where it changes from forced to free modes at (r_c). However, there exists an unrealistic jump discontinuity in the vorticity field. While vorticity remains constant inside the core, it drops abruptly to zero at (r_c), and remains zero for the rest of the interval [r_c , ∞). In reality however it should be a smooth transition of vorticity profile from forced vortex to free vortex.

Burger's (1948) tangential velocity provides a continuous transition for the vorticity at r_c. The vortex model assumes the radial velocity to vary linearly with the radius. This model produced an improvement between the predicted and observed values of tangential velocity near the core. The assumed radial and axial velocity components do satisfy the equations of continuity, radial and axial momentum. However, the radial velocity varies linearly with the radius making it unbounded for the case of unconfined whirls.

Scully (1975) proposed an empirical formula for the tangential velocity, which has also a smooth transition for the vorticity at the core radius. He assumed non-zero radial and axial velocity distributions. But, the calculated values of tangential velocity near the core radius are far from the observed laminar eddies.

All vortex models are single cell vortices. Sullivan (1959) proposed a new vortex formulation where radial and axial velocity components reverse their directions near center of vortex thus producing a central recirculation zone. This type of vortex is known as two-celled vortex. Alike to Burgers the radial velocity is unbounded as $r \to \infty$.

Vatistas et al. (1991) proposed a new tangential velocity formula. Based on theoretical and experimental study on concentrated vortex in vortex chamber, they showed that the azimuthal velocity component does not depend strongly on the axial direction Vatistas et al. (1986). By using this, the new family of tangential profiles the radial velocity component deduced from θ-momentum equation while the axial velocity component was determined from continuity. Depending upon the value of the exponent (n), one can obtain tangential velocity distributions from Rankine (1858) to Scully (1975)

vortex models. All velocity distributions for this model are finite for any r for all the values of exponent n except for $n < 1$. Further studies by Vatistas (1998) produced a new vortex model, capable of generating profiles ranging from jet-like to wake–like shapes. With proper choice of scaling constant, one could also develop a single cell or double cell vortex. The steady state vortex flow can be converted into time decaying vortex flow with proper choice of transformations under assumptions of incompressible, intense vortex flow Vatistas and Aboelkassem (2005). Through this technique, steady state solutions can also be recovered from time–decaying vortices and *vise versa*.

The temperature separation in vortex tubes is known to the technical and scientific communities since the early 19 hundreds from the work of Ranque (1933) and Hilsch (1947). Although its causality has yet to be completely resolved, the manifestations, design, and *modus operandi* of the device are simple to understand and apply. In fact numerous mechanical components are presently spot-cooled using vortex tubes. The main part of the devise is an ordinary pipe of circular cross-section. Compressed air is admitted tangentially into the tube, from the side pipe wall, at high velocity whereby the entering flow splits into two streams. One of the streams exits the confinement through a central circular orifice located at one end of the tube, with a temperature considerably lower than it had at the inlet. The other leaves the pipe from the opposite end via a peripheral annular slit, with a temperature much higher than the inlet. The general thermal effect however, as it will be shown latter, is not exclusive to the specific engineering application, the vortex tube.

2 Previous work and thesis objectives

2.1 Previous work

For most of the vortices encountered in science and engineering the flow could be assumed as incompressible. However, there are instances where density changes as a result of fluid motion cannot be neglected. Tailor (1930) presented a theoretical paper on isentropic potential vortex where he considered effects of compressibility. Sibulking (1962) performed an unsteady analysis for the flow development inside vortex tubes. The temperature and velocity were calculated as a function of radius. Mack (1960) studied the compressible laminar, vortex flow created inside a rotating cylinder considering a perfect, heat conducting gas.

Aboelkassem and Vatistas (2007) extended the previous work of Vatistas and et al. (1991) incompressible vortices into compressible. Density variation in mathematical formulation of governing equations was included via the energy and state equations. The governing equations were simplified based on order of magnitude analysis performed by Aboelkassem and Vatistas (2007). Then using the analogy between incompressible and compressible flow, and upon renormalization, all the velocity components from incompressible flow became applicable also to compressible vortex category. The temperature variation was calculated from the energy equation, while the density and pressure changes were obtained from the radial momentum and the equation of state respectively. The radial and axial velocity components contain dimensionless density (β) were affected by change in density, whereas tangential velocity form, contains no

density term and thus should remain the same. Taking the Prandtl Number equal to 2/3, an exact solution of energy equations was found.

The results also proved that there are very small changes in temperature values for Prandtl numbers ranging from (0.680-0.716). The temperature, density, and pressure decrease as the flow converges from far towards center of the vortex. It was also found that the previous flow properties decrease with the vortex Mach number.

As discussed previously, solutions to laminar incompressible and compressible vortex flows were possible due to the abundance of previous work on this subject matter. Turbulent vortex flows however are comparatively more complex than laminar. Ramasamy and Leishman (2006) studied turbulent helicopter tip vortices and found that these to be laminar inside core. Flow transition was observed when a critical vortex Reynolds number was reached. The flow changes entirely to turbulent flow at a second critical Reynolds number. In this region the tangential velocity decreases at a slower pace as compared to laminar, which leads to the conclusion that turbulent vortices cannot be modeled using the previous methods.

Vatistas (2006) included the effects of turbulence by modifying the original laminar tangential velocity (for n=2) formula. The value of a new exponent in the proposed tangential velocity formula was obtained by the least square method. The new turbulent model approximated fairly the experimental result of Ramasamy and Leishman (2006).

Among the vortex flow applications is also the vortex tube. Ranque (1933) was the first who discovered the energy separation phenomenon by injecting tangentially a

pressurized gas into a cylindrical tube pipe. The term “energy separation” here means that the flow segregates into two flow regions; one sector is hot (its static temperature is higher than the inlet) while the other is cold (its temperature is lower than the inlet). Ranque came to the conclusion that expansion and compression of the gas is the main reason for the energy separation. Hilsch (1947) produced a more efficient design of the tube. He reported that internal friction is the main reason behind “energy separation” which causes the transfer of heat from core to outer region and thus cooling down of gas in core and heats up the gas in the peripheral region. The vortex tube became also known with name of its two invertors (Ranque- Hilsch tube).

Deissler and Perlmutter (1960) published a theoretical paper on turbulent compressible vortex flow and pointed out that the shear work, done by or on fluid element, is the main cause behind the separation. Based on observations many researchers proposed various theories about the origin of the phenomenon. However no one gave a concrete account of the event. Due to this reason the cause became so mysterious that some called upon Maxwell’s demon to resolve the impasse. The most recent attempt to explain the cause is by Liew and Zeegers (2012). They argued that as a gas packet moves towards the region of higher pressure it compresses, causing an increase in temperature near to wall of vortex tube. If the fluid element moves instead towards lower pressure region (towards the core), it becomes cooler due to its expansion. They also assumed that both expansion and compression of fluid element is very fast and there is no time for heat transfer between fluid elements and their surroundings and thus the process is adiabatic.

The theories mentioned above tried to explain the cause of energy separation in

confined vortices (such as in vortex tubes). The energy separation phenomenon has also been found in unconfined vortices such as in tornadoes and interaction of vortices with shock waves Katz (1960), Cattafesta and Settles (1992) respectively. Therefore, the main thermal event is not exclusive to vortex tubes.

Work on simple formulations for steady turbulent, compressible vortices is nonexistent. The only papers that we were able to locate in the open literature were those of Grasso and Pirozzoli (1999) and Pirozzoli et al (1999) concerning decaying and starting turbulent compressible vortices respectively.

2.2 Thesis Objectives

In present study, we extended the previous work of Aboelkassem and Vatistas (2007) on the laminar compressible into turbulent compressible vortex flow. The effects of turbulence were captured by introducing the modified tangential velocity formula of Vatistas (2006). The radial and axial velocity components were derived from tangential - momentum and conservation of mass equations respectively. The solution of energy equation under laminar and turbulent flow conditions was obtained for any value of Prandtl number ranging from 0.680 (Helium) to 0.716 (Nitrogen) using numerical integration embedded in Matlab's routine quadl (adaptive Lobatto quadrature within an error of 10^{-6}).

The temperature is then used to calculate the radial distribution of density and pressure using radial-momentum equation and equation of state respectively. The effects of Prandtl number on solution of the energy equation were also tested. The numerical results are also shown to respect the second law of thermodynamics.

The novel approach is then used to explain the mysterious energy separation phenomenon that causes the thermal effect. It was found that this is due to the competition between the heating up of the gas generated by friction, and cooling down due to its expansion as it moves towards the region of decreasing pressure. Past study of the tornadoes also reveals this thermal effect and the same methodology also explains its cause. Thus, in present study, we also considered unconfined vortex flow in order to support the reason behind this effect.

3 The Governing Flow Equations

3.1 Laminar Compressible Vortex Flow

Consideration is given here to general form of the conservation of mass and momentum equations for an isolated vortex, when the fluid properties are assumed not to depend strongly on temperature. Moreover, the flow field is considered to be steady, compressible, and axisymmetric where gravity is neglected. Under these conditions the conservation equations take the following simpler form**,**

Conservation of Mass

$$\frac{\partial(\rho V_r)}{\partial r}+\frac{\partial(\rho V_z)}{\partial z}+\frac{\rho V_r}{r}=0$$

Radial Momentum

$$\left[V_r\frac{\partial V_r}{\partial r}-\frac{V_\theta^2}{r}\right]=-\frac{1}{\rho}\frac{\partial p}{\partial r}+\frac{\mu}{\rho}\left[\frac{\partial^2 V_r}{\partial r^2}+\frac{1}{r}\frac{\partial V_r}{\partial r}-\frac{V_r}{r^2}+\frac{1}{3}\frac{\partial}{\partial r}\left(\frac{\partial V_r}{\partial r}+\frac{\partial V_z}{\partial z}+\frac{V_r}{r}\right)\right]$$

Tangential Momentum

$$V_r\frac{\partial V_\theta}{\partial r}+\frac{V_r V_\theta}{r}=\frac{\mu}{\rho}\left[\frac{\partial^2 V_\theta}{\partial r^2}+\frac{1}{r}\frac{\partial V_\theta}{\partial r}-\frac{V_\theta}{r^2}\right]$$

Axial Momentum

$$V_r\frac{\partial V_z}{\partial r}+V_z\frac{\partial V_z}{\partial z}=-\frac{1}{\rho}\frac{\partial p}{\partial z}+\frac{\mu}{\rho}\left[\frac{\partial^2 V_z}{\partial r^2}+\frac{1}{r}\frac{\partial V_z}{\partial r}+\frac{\partial^2 V_z}{\partial z^2}+\frac{1}{3}\frac{\partial}{\partial z}\left(\frac{\partial V_r}{\partial r}+\frac{\partial V_z}{\partial z}+\frac{V_r}{r}\right)\right]$$

Interest is now focused on the classical solutions where the total velocity vector has the form:

$$q\left[V_r(r),V_\theta(r),V_z=zfn(r)\right]$$

Where the variables are explained in the nomenclature and the coordinate system is given in Figure 3.1.

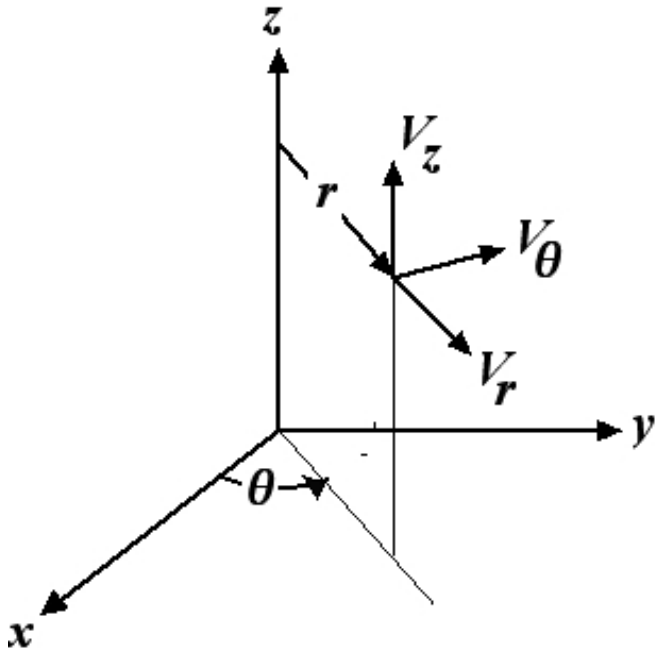

Figure 3.1 Definition of the coordinate system.

Using the dimensionless form of the variables, Aboelkassem and Vatistas (2007):

$$V_r = uV_{\theta max}$$

$$V_\theta = VV_{\theta max}$$

$$V_z = \zeta hV_{\theta max}$$

$$\rho = \beta\rho_\infty$$

$$r = \xi r_c$$

$$p = \Pi\rho_\infty V_{\theta max}^2$$

$$Re = \frac{\rho_\infty V_{\theta max} r_c}{\mu}$$

$$T = T_\infty\Theta$$

$$z = \zeta r_c \qquad \text{(A)}$$

and furthermore considering a strong vortex flow, in which both the radial and axial velocity components are very small (order of magnitude of δ) as compared to the tangential velocity component, the dimensionless conservation of mass and momentum equations are, Aboelkassem and Vatistas (2007):

Conservation of Mass

$$\underset{\delta}{\frac{\partial(\beta u)}{\partial\xi}} + \underset{\delta}{\beta h} + \underset{\delta}{\frac{\beta u}{\xi}} = 0 \qquad (3.1.1)$$

Note that all the terms in the conservation of mass have same order of magnitude. Therefore, the equation remains the same**.**

Radial momentum

$$u\frac{\partial u}{\partial \xi} - \frac{V^2}{\xi} = -\frac{1}{\beta}\frac{\partial \Pi}{\partial \xi} + \frac{1}{Re\beta}\left[\frac{4}{3}\left(\frac{\partial^2 u}{\partial \xi^2} + \frac{1}{\xi}\frac{\partial u}{\partial \xi} - \frac{u}{\xi^2}\right) + \frac{1}{3}\frac{\partial^2 (h\zeta)}{\partial \zeta \partial \xi}\right]$$

$$\delta \quad \delta \quad 1 \qquad 1 \qquad \delta \qquad \delta \qquad \delta \quad \delta \qquad \delta$$

The radial momentum equation contains two terms having order of magnitude 1. Neglecting the terms of order δ or smaller yields:

$$\frac{\partial \Pi}{\partial \xi} = \frac{\beta V^2}{\xi} \tag{3.1.2}$$

A similar procedure can be implemented on tangential and axial momentum equations.

Tangential momentum

$$Re\beta\left[u\frac{\partial V}{\partial \xi} + \frac{uV}{\xi}\right] = \frac{\partial^2 V}{\partial \xi^2} + \frac{1}{\xi}\frac{\partial V}{\partial \xi} - \frac{V}{\xi^2}$$

$$\frac{1}{\delta} \qquad \delta \quad 1 \quad \delta \, 1 \qquad 1 \qquad 1 \quad 1$$

or

$$Re\beta\left[u\frac{\partial V}{\partial \xi} + \frac{uV}{\xi}\right] = \frac{\partial^2 V}{\partial \xi^2} + \frac{1}{\xi}\frac{\partial V}{\partial \xi} - \frac{V}{\xi^2} \tag{3.1.3}$$

Axial momentum

$$u\frac{\partial(\zeta h)}{\partial\xi}+\zeta h^2=-\frac{1}{\beta}\frac{\partial\Pi}{\partial\zeta}+\frac{1}{Re\beta}\left[\frac{\partial^2(\zeta h)}{\partial\xi^2}+\frac{1}{\xi}\frac{\partial(\zeta h)}{\partial\xi}+\frac{\partial^2(\zeta h)}{\partial\zeta^2}+\frac{1}{3}\frac{\partial}{\partial\zeta}\left(\frac{\partial u}{\partial\xi}+h+\frac{u}{\xi}\right)\right]$$

$\delta \quad \delta \quad \delta^2 \qquad 1 \quad \delta \quad \delta \qquad \delta \qquad \delta \qquad \delta \quad \delta \quad \delta$

Therefore

$$\frac{\partial\Pi}{\partial\zeta}\approx 0 \tag{3.1.4}$$

From the axial momentum equation the conclusion is that the dimensionless static pressure does not vary in the axial direction. Therefore, the pressure must be only a function of ξ, and the partial derivative in equation (3.1.2), changes into total.

$$\frac{d\Pi}{d\xi}=\frac{\beta V^2}{\xi} \tag{3.1.5}$$

It is also clear from continuity and the momentum equations that there are five unknowns (u, V, h, β, Π) and only four equations to solve. Therefore, in order to determine the unknowns, one more equation is required. The extra equation will be the equation of state.

The gas is assumed to be calorically perfect $\left(c_p, c_v, \mu, k, \gamma\right)$. The equations on the thermal side are:

The equation of state and energy equation in dimensional form are given as follow:

Equation of State

$$p = \rho RT$$

Energy Equation

$$\frac{1}{r}\frac{d}{dr}\left(k\,r\frac{dT}{dr}\right) + \Phi = \rho c_p V_r \frac{dT}{dr} - V_r \frac{dp}{dr}$$

Where Φ, is the dissipation function, given by,

$$\Phi = 2\mu\left[\left(\frac{\partial V_r}{\partial r}\right)^2 + \left(\frac{V_r}{r}\right)^2 + \left(\frac{\partial V_z}{\partial z}\right)^2 + \frac{1}{2}\left(\frac{\partial V_\theta}{\partial r} - \frac{V_\theta}{r}\right)^2 + \right.$$
$$\left. + \frac{1}{2}\left(\frac{\partial V_z}{\partial r}\right)^2 - \frac{1}{3}\left(\frac{\partial V_r}{\partial r} + \frac{V_r}{r}\right)^2\right]$$

In dimensionless form with the order of magnitude designation of the state and energy equations are Aboelkassem and Vatistas (2007):

State Equation

$$\Pi = \frac{\beta\Theta}{\gamma M_0^2} \qquad (3.1.6)$$

1 1

Energy Equation

$$\underset{1}{\frac{kT_\infty}{r_c^2\xi}\frac{d}{d\xi}\left(\xi\frac{d\Theta}{d\xi}\right)}+\underset{\frac{1}{\delta}\,\delta}{\Phi}=\underset{1}{\beta PrReu\left(\frac{kT_\infty}{r_c^2}\right)\frac{d\Theta}{d\xi}}-\underset{\frac{1}{\delta}}{\frac{kT_\infty}{r_c^2}PrRe(\gamma-1)M_0^2u\frac{d\Pi}{d\xi}}\qquad\qquad\delta \tag{3.1.7}$$

Using the order of magnitude, the dissipation function is:

$$\Phi=2\mu\Bigg[\underset{\delta^2}{\left(\frac{V_{\theta max}}{r_c}\right)^2\left(\frac{\partial u}{\partial\xi}\right)^2}+\underset{\delta^2}{\left(\frac{V_{\theta max}}{r_c}\right)^2\left(\frac{u}{\xi}\right)^2}+\underset{\delta^2}{\left(\frac{V_{\theta max}}{r_c}\right)^2h^2}+\underset{1\quad 1}{\frac{1}{2}\left(\frac{V_{\theta max}}{r_c}\right)^2\left(\frac{\partial V}{\partial\xi}-\frac{V}{\xi}\right)^2}$$
$$+\underset{\delta^2}{\frac{1}{2}\left(\frac{V_{\theta max}}{r_c}\right)^2\zeta^2\left(\frac{\partial h}{\partial\xi}\right)^2}-\underset{\delta^2}{\frac{1}{3}\left(\frac{V_{\theta max}}{r_c}\right)^2\left(\frac{\partial u}{\partial\xi}+h+\frac{u}{\xi}\right)^2}\Bigg]$$

Neglecting terms of δ or higher yields:

$$\Phi=\mu\frac{V_{\theta max}^2}{r_c^2}\left(\frac{dV}{d\xi}-\frac{V}{\xi}\right)^2$$

$$\Phi=Pr\,M_o^2(\gamma-1)\left(\frac{k\,T_\infty}{r_c^2}\right)\left[\xi^2\left\{\frac{d}{d\xi}\left(\frac{V}{\xi}\right)\right\}^2\right]$$

$$\Phi=Pr\,M_o^2(\gamma-1)\left(\frac{k\,T_\infty}{r_c^2}\right)f$$

Inserting the above expressions of Φ and $\frac{d\Pi}{d\xi}$ in equation (3.1.7) gives,

$$\frac{1}{\xi}\frac{d}{d\xi}\left(\xi\frac{d\Theta}{d\xi}\right)+\Pr\left(\gamma-1\right)M_0^2 f=\beta\Pr Reu\frac{d\Theta}{d\xi}-\Pr Re\left(\gamma-1\right)M_0^2 u\frac{\beta V^2}{\xi} \tag{3.1.8}$$

Taking $U=\beta Reu$ and $H=\beta Reh$ yields:

Conservations of Mass:

$$\frac{1}{\xi}\frac{d}{d\xi}\left(U\xi\right)+H=0 \tag{3.1.9}$$

Radial momentum

$$\frac{d\Pi}{d\xi}=\frac{\beta V^2}{\xi} \tag{3.1.10}$$

Tangential momentum

$$\frac{U}{\xi}\frac{d}{d\xi}\left(V\xi\right)=\frac{d}{d\xi}\left[\frac{1}{\xi}\frac{d}{d\xi}\left(V\xi\right)\right] \tag{3.1.11}$$

Energy Equation

$$\frac{1}{\xi}\frac{d}{d\xi}\left(\xi\frac{d\Theta}{d\xi}\right)-\Pr U\frac{d\Theta}{d\xi}=-\Pr\left(\gamma-1\right)M_0^2\left(f+\frac{UV^2}{\xi}\right) \tag{3.1.12}$$

Equation of State

$$\Pi=\frac{\beta\Theta}{\gamma M_0^2} \tag{3.1.13}$$

3.2 Turbulent Compressible Vortex Flow

The general form of the conservation of mass, the three momentum equations, equation of state, and energy equation that were derived in section (3.1) remain the same for turbulent compressible vortex flow. The effects of turbulence are roughly approximate using the effective viscosity, whereby the molecular viscosity (υ_{mol}) is augmented by a constant eddy viscosity (υ_{eddy}) component.

The experiments of Ramasamy and Leishman (2006) on helicopter blade tip vortices revealed that in the case of turbulent flow, the rate of decrease in the tangential velocity profile (outside the core) is smaller than the laminar. Thus, the tangential velocity profile is shifted upwards as the flow becomes turbulent. Also there are five equations containing six unknowns. Therefore, the system is undetermined. In order to close this system, one variable must be assumed and the rest could be found using the conservations equations.

To account for the effect of turbulence, the tangential velocity of Vatistas (2006) for a turbulent vortex was used:

$$V = \frac{V_\theta}{V_{\theta\max}} = \xi\left(\frac{a+1}{a+\xi^4}\right)^m \qquad (3.2.1)$$

This dimensionless tangential velocity (V) must attain a maximum at ξ = 1 which requires that $m = \frac{a+1}{4}$. The tangential velocity for the laminar vortex case (n=2) can be recovered by setting a = 1. The degree of turbulence is defined by the scaling constant (a); as a decreases turbulence level increases. The last constant is evaluated by curve

fitting equation (3.2.1) to the experimental values via the least square method,

$$E = \sum_{j=1}^{N} \left[V_j - \xi_j \left(\frac{a+1}{a+\xi_j{}^4} \right)^{\frac{a+1}{4}} \right]^2$$

Where V_j is the experimental velocity value at the discrete point ξ_j. The average value for the dataset given in Figure 3.2 was found to be 0.7. The velocity of a turbulent vortex (a = 0.7) is seen to lift up from the laminar profile (a = 1.0). The vortex of Han et al. (1997) is laminar and incompressible. The vortices of Ramasamy and Leishman (2006) and Koval and Michaelov (1972) are turbulent and incompressible. The rest represent turbulent compressible vortices with Mach numbers ranging from 0.48 in Kalhoran and Smart **(**2000) to 0.98 in Pivirotto (1966)**.** Because, the incompressible turbulent vortex of Ramasamy and Leishman (2006) and Koval and Michaelov (1972) correlate well with the compressible group, density variations seem not to affect the tangential velocity to a great degree. The last was previously proposed by Aboelkassem and Vatistas (2007).

The radial velocity U is derived using the tangential momentum equation and is given by,

$$U = -\left[\frac{4b_1 m\xi^7}{b_1\xi^8 + b_2\xi^4 + b_3} + \frac{12am\xi^3}{b_1\xi^8 + b_2\xi^4 + b_3} \right] \qquad (3.2.2)$$

Where $b_1 = -(2m-1); b_2 = -2a(m-1); b_3 = a^2$.

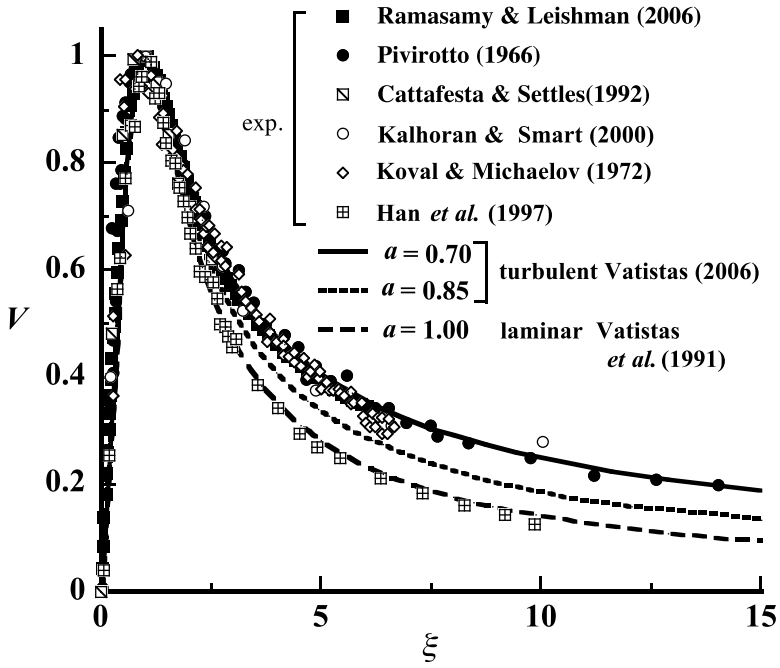

Figure 3.2 Dimensionless tangential velocity profiles for laminar and turbulent vortices.

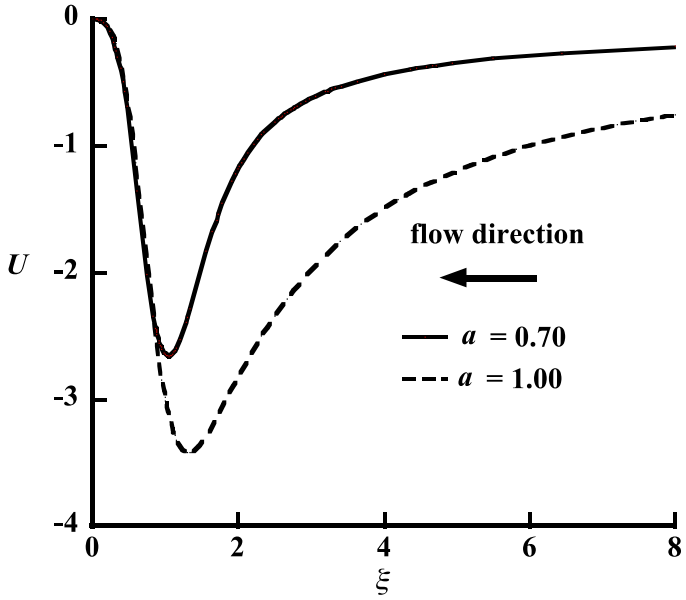

Figure 3.3 The radial velocity distribution for laminar and turbulent vortices.

The Figure3.2 illustrates the dimensionless tangential velocity profiles for laminar and turbulent vortices. Parameter a = 0.7 is found via the least squares method, curve fitting of equation (3.2.1) to the cumulative experimental data points shown in this figure, excluding of course the data of Han et al, (1997). The velocity of a turbulent vortex (a = 0.7) is seen to lift up from the laminar profile (a = 1.0). Except the vortices of Ramasamy and Leishman (2006) and Koval and Michaelov (1972) the rest are compressible turbulent vortices with Mach numbers ranging from 0.48 in Kalhoran and Smart (2000) to 0.98 in Pivirotto (1966). Because, the incompressible turbulent vortices in Ramasamy and Leishman (2006) and Koval and Michaelov (1972) correlate well with the compressible group, density variations do not seem to affect the tangential velocity to a great degree.

The Figure 3.3 shows the radial velocity distribution for laminar and turbulent vortices. The velocity components in both cases are everywhere negative indicating that the radial flow is converging towards the center.

The axial velocity H is determined from conservation of mass,

$$H = \left[\frac{16b_1b_2m\xi^{10} + 32b_1b_3m\xi^{6} + 48amb_3\xi^{2} - 48amb_1\xi^{10}}{\left(b_1\xi^{8} + b_2\xi^{4} + b_3\right)^{2}} \right] \qquad (3.2.3)$$

3.3 The Boundary Conditions

The equations derived in sections (3.1) and (3.2) require boundary conditions these are:

(i) $\xi = 0$ $\qquad V = 0, U = 0, \frac{d\Theta}{d\xi} = 0, \frac{dH}{d\xi} = 0$

(ii) $\xi \to \infty$ $\qquad \left(\Theta, \beta, \gamma M_0^2 \Pi\right) \to 1$

4 Numerical Solution

The energy equation derived in the chapter 3 is an ordinary, second order, linear differential equation (that requires 2-boundary conditions). For the laminar case, it can be solved analytically by taking Pr =2/3. Its exact solution can be found in Appendix A. As for as the turbulent vortex flow is concerned, the energy equation cannot be solved analytically.

Moreover, exact solution of the energy equation under laminar flow assumption is not known analytically for Pr numbers other than 2/3. Therefore, numerical integration is adopted to solve the energy, valid for any Pr number, for both laminar and turbulent flows.

4.1 Numerical Method Applied on Energy Equation under Laminar Flow assumption

The simplified equations (3.1.9), (3.1.10), and (3.1.11) for the laminar compressible vortex flow have exactly the same forms as those for incompressible vortices, Vatistas and Aboelkassem (2005)**.**Using the analogy between incompressible (*n*=2) and compressible vortices U, V and H for laminar compressible vortex are as follows:

$$U = \frac{-6\xi^3}{1+\xi^4} \quad ; \quad V = \frac{\sqrt{2}\,\xi}{\sqrt{1+\xi^4}} \; ; \quad H = \frac{24\xi^2}{\left(1+\xi^4\right)^2} \; ; f = \frac{4\xi^8}{\left(1+\xi^4\right)^3}$$

The energy equation is given by (3.1.12)

$$\frac{1}{\xi}\frac{d}{d\xi}\left[\xi\frac{d\Theta}{d\xi}\right] - PrU\frac{d\Theta}{d\xi} = -Pr(\gamma - 1)M_0^2\left[f + \frac{UV^2}{\xi}\right]$$

Multiply both sides of energy equation by (ξ) we obtain,

$$\frac{d}{d\xi}\left[\xi\frac{d\Theta}{d\xi}\right] - PrU\xi\frac{d\Theta}{d\xi} = -Pr(\gamma - 1)M_0^2\left[f\xi + UV^2\right]$$

Let $Y = \xi\frac{d\Theta}{d\xi}$

Above equation becomes

$$\frac{dY}{d\xi} - PrUY = -Pr(\gamma - 1)M_0^2\left(f\xi + UV^2\right) \tag{4.1.1}$$

The integrating factor (λ) for the above equation is:

$$\lambda = \exp\left(-\int_0^{\xi} PrU d\xi\right) \tag{4.1.2}$$

Equation (4.1.1) can then be rewritten as follow:

$$d(Y\lambda) = -Pr(\gamma - 1)M_0^2\left(f\xi + UV^2\right)\lambda d\xi$$

Integration of above equation along with boundary condition at vortex center (the derivative of Θ is zero) yields the change of temperature with the radius,

$$\frac{d\Theta}{d\xi} = -Pr(\gamma - 1)M_0^2\frac{\int_0^{\xi}\left(f\xi + UV^2\right)\lambda d\xi}{\xi\lambda} \tag{4.1.3}$$

The variation of temperature with the radius is obtained by integrating the previous equation once more, and implementing the additional boundary condition that requires that far away from vortex center, Θ should approach asymptotically its ambient value of one.

After some straightforward mathematical manipulations the following equation for the temperature is obtained,

$$\Theta_{\xi} = -\Pr(\gamma - 1)M_0^2 \int_0^{\xi} \frac{\int_0^{\xi} \left(f\xi + UV^2\right)\lambda d\xi}{\xi\lambda} d\xi + \Pr(\gamma - 1)M_0^2 \int_0^{\infty} \frac{\int_0^{\xi} \left(f\xi + UV^2\right)\lambda d\xi}{\xi\lambda} d\xi + 1 \tag{4.1.4}$$

Expression (4.1.4) is a generalized equation derived from the energy equation (3.1.12) valid for both laminar and turbulent compressible vortex.

The final form of the integrating factor (λ) is obtained by inserting the value of U in equation (4.1.2),

$$\lambda = \left(1 + \xi^4\right)^{\frac{3\Pr}{2}} \tag{4.1.5}$$

This is the final form of λ valid for the linear differential equation (3.1.12) under laminar flow conditions.

4.2 Numerical Method Applied on Energy Equation under Turbulent Flow assumption

The integrating factor (λ) for the turbulent vortex is obtained by inserting the expression of U from equation (3.2.2) in (4.1.2),

$$\lambda = \exp\left(\int_0^{\xi} \frac{4b_1 mPr\xi^7}{b_1\xi^8 + b_2\xi^4 + b_3} d\xi + \int_0^{\xi} \frac{12amPr\xi^3}{b_1\xi^8 + b_2\xi^4 + b_3} d\xi\right)$$

$$\lambda = \exp\left(I_1 + I_2\right) \tag{4.2.1}$$

Where $I_1 = \int \frac{4b_1 mPr\xi^7}{b_1\xi^8 + b_2\xi^4 + b_3} d\xi$; $I_2 = \int \frac{12amPr\xi^3}{b_1\xi^8 + b_2\xi^4 + b_3} d\xi$

The Integral $\left(I_1 \text{ and } I_2\right)$ are solved separately as follow:

$$I_1 = \int \frac{4b_1 mPr\xi^7}{b_1\xi^8 + b_2\xi^4 + b_3} d\xi$$

Inserting $\xi^4 = t$, $d\xi = \frac{dt}{4\xi^3}$ in above equation and by simple mathematical manipulations gives the following expression of $\left(I_1\right)$,

$$I_1 = b_1 mPr \int \frac{t}{b_1 t^2 + b_2 t + b_3} dt$$

$$I_1 = \ln\left\{\frac{\left(b_1 t^2 + b_2 t + b_3\right)^{\frac{1}{2b_1}}}{\left(\frac{2b_1 t + b_2 - \sqrt{b_2^2 - 4b_1 b_3}}{2b_1 t + b_2 + \sqrt{b_2^2 - 4b_1 b_3}}\right)^{\frac{b_2}{2b_1\sqrt{b_2^2 - 4b_1 b_3}}}}\right\}^{b_1 mPr}$$

Putting back $t = \xi^4$ in above equation yields,

$$I_1 = \ln\left\{ \frac{\left(b_1\xi^8 + b_2\xi^4 + b_3\right)^{\frac{1}{2b_1}}}{\left(\frac{2b_1\xi^4 + b_2 - \sqrt{b_2^{\,2} - 4b_1b_3}}{2b_1\xi^4 + b_2 + \sqrt{b_2^{\,2} - 4b_1b_3}}\right)^{\frac{b_2}{2b_1\sqrt{b_2^{\,2}-4b_1b_3}}}} \right\}^{b_1 mPr} \tag{4.2.2}$$

The same procedure can be applied to find the second integral $\left(I_2\right)$ and is given by,

$$I_2 = \ln\left(\frac{2b_1\xi^4 + b_2 - \sqrt{b_2^{\,2} - 4b_1b_3}}{2b_1\xi^4 + b_2 + \sqrt{b_2^{\,2} - 4b_1b_3}}\right)^{\frac{3amPr}{\sqrt{b_2^{\,2}-4b_1b_3}}} \tag{4.2.3}$$

Inserting the values of (4.2.2) and (4.2.3) in (4.2.1) we obtain:

$$\lambda = \left(\frac{2b_1\xi^4 + b_2 - \sqrt{b_2^{\,2} - 4b_1b_3}}{2b_1\xi^4 + b_2 + \sqrt{b_2^{\,2} - 4b_1b_3}}\right)^{\frac{3amPr}{\sqrt{b_2^{\,2}-4b_1b_3}}} \left(\frac{\left(b_1\xi^8 + b_2\xi^4 + b_3\right)^{\frac{1}{2b_1}}}{\left(\frac{2b_1\xi^4 + b_2 - \sqrt{b_2^{\,2} - 4b_1b_3}}{2b_1\xi^4 + b_2 + \sqrt{b_2^{\,2} - 4b_1b_3}}\right)^{\frac{b_2}{2b_1\sqrt{b_2^{\,2}-4b_1b_3}}}} \right)^{b_1 mPr}$$

The above expression is the integrating factor of the linear differential equation (3.1.12) under turbulent vortex flow conditions.

5 Implementation of the Matlab Code

In the last chapter, the integrating factor (λ) was derived for any Prandtl number for the energy under the assumption of laminar and turbulent compressible vortex flows. Equation (4.1.4) is general and thus applicable to both laminar and turbulent vortices. Note that the two flows have different expressions for (U, V, f, λ). Equation (4.1.4) is solved using numerical integration routine quadl (adaptive Lobatto quadrature within an error of 10^{-6}) embedded in Matlab.

In order to solve energy equation numerically, the entire domain of the independent variable (ξ) is divided into small parts. To determine the integrand more accurately, the midpoint rule of numerical integration is used where the integrand is calculated at the center of each part. This value gives the height of the function and multiply with the step size $\left(h = \frac{\xi_\infty}{\text{No. of Parts}} \right)$ provides the area under the curve. The Matlab Code script file could be found in Appendix B.

5.1 Verification of Matlab Code

It was mentioned in chapter 4, that the energy equation for laminar compressible vortex, valid for Pr=2/3, has exact solution **.**This is,

$$\Theta_{\text{Exact Solution}} = 1 + \frac{1}{6}(\gamma - 1) M_0^2 \left[\tan^{-}\left(\xi^2\right) - \frac{\xi^2}{1+\xi^4} - \frac{\pi}{2} \right] \tag{5.1.1}$$

The detailed derivation for the exact solution of energy equation is given in Appendix A.

The Code is first implemented to solve the energy equation under laminar flow conditions for Pr =2/3. The results from the two approaches (exact and numerical) are compared on Table 5.1:

Table 5-1 Comparison of exact solution of energy equation under laminar flow condition with numerical solution for Pr=2/3, ξ_∞ =200 and number of nodes=20,000.

	$M_0 = 0.5$		$M_0 = 1.0$	
ξ	Θ (Exact)	Θ (Numerical)	Θ (Exact)	Θ (Numerical)
0	0.97382	0.973821	0.89528	0.895284
0.5	0.973981	0.973982	0.895926	0.895929
1	0.978577	0.978577	0.914307	0.91431
1.5	0.986844	0.986845	0.947376	0.94738
2	0.991995	0.991996	0.967982	0.967985
2.5	0.994756	0.994756	0.979023	0.979026
3	0.996326	0.996327	0.985306	0.985309
3.5	0.997291	0.997292	0.989164	0.989167
4	0.997922	0.997923	0.991688	0.991692
4.5	0.998357	0.998357	0.993426	0.99343
5	0.998668	0.998669	0.994672	0.994676

The required values used to perform the calculations are: Pr =2/3, Mo = 0.5, ξ_∞ = 200 and number of nodes = 20,000. The exact and numerical solutions are seen to match up to fifth decimal place. This confirms the adequacy of the Matlab code in obtaining acceptable numerical solution for the problem under consideration.

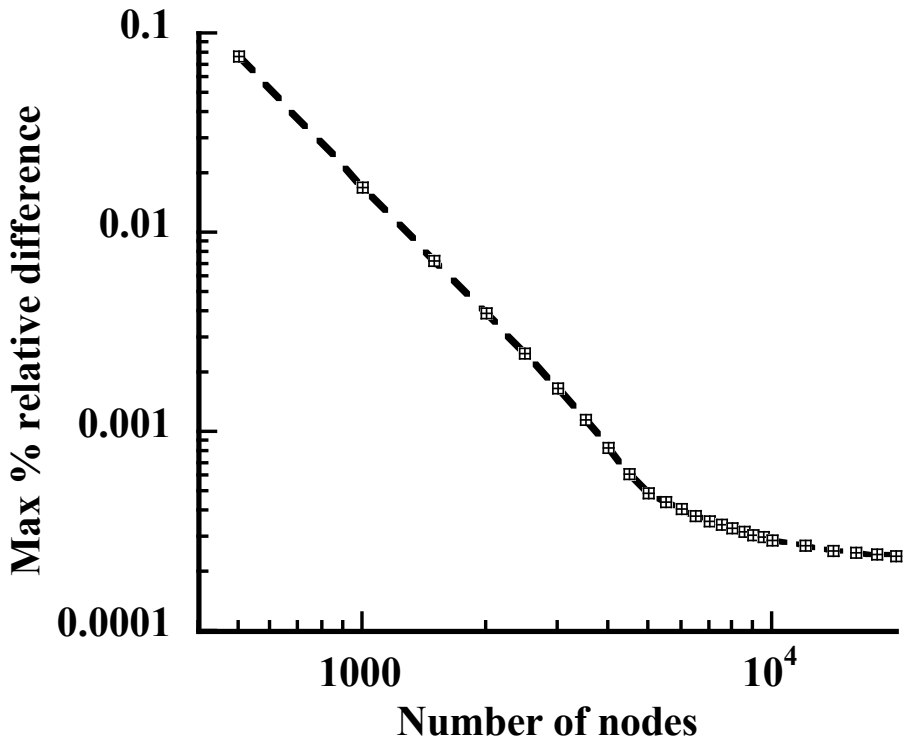

Figure 5.1 Maximum absolute relative percentage difference between the numerical and exact solution of the energy equation under laminar flow condition with M_0=0.8,Pr=2/3 and $\xi_\infty = 200$.

We will explain later why infinity was assumed to be 200 times core radii. We took number of nodes equals to 20,000.In order to explain this, an experiment was conducted by calculating the maximum absolute relative percentage error between the numerical and exact solution of the energy equation.

Figure 5.1 shows that the maximum absolute relative percentage error decreases by increasing the number of nodes. The error becomes insignificant as number of nodes reaches 20,000.

6 Results for Laminar Compressible Vortex Flow

6.1 Calculation of Density and Pressure

The temperature values, obtained through numerical integration of Eq. (4.1.4), are then employed to calculate the density and pressure using equations (14) and (6) of Vatistas and Aboelkassem (2006) respectively,

$$\beta = \frac{\exp\left[\gamma M_0^2 \left\{\int_0^{\xi} \frac{V^2}{\xi\Theta} d\xi - \int_0^{\infty} \frac{V^2}{\xi\Theta} d\xi\right\}\right]}{\Theta} \tag{6.1.1}$$

$$\Pi = \frac{\exp\left[\gamma M_0^2 \left\{\int_0^{\xi} \frac{V^2}{\xi\Theta} d\xi - \int_0^{\infty} \frac{V^2}{\xi\Theta} d\xi\right\}\right]}{\gamma M_0^2} \tag{6.1.2}$$

6.2 Effect of Prandtl Number

The effect of Prandtl number is also examined here. The Prandtl number for most of the gases at one atmosphere and 300 K varies from 0.680 (Helium) to 0.716 (Nitrogen). The influence that the Pr number has on temperature is tested for $M_0 = 0.8$ and $\xi_\infty = 200$. If one takes the Pr =2/3 for air instead of 0.707, the results presented on Table 6.1 show that the maximum deviation occurs at vortex center and is less than 0.5%.

Moreover, if we take the Pr =2/3 for Nitrogen (where actual value of Pr=0.716) to calculate the temperature, the maximum percentage difference is found to be less than 0.6%. It is clear from the tabulated results that there are very small changes in

temperature profile as a result of modest changes in Pr numbers. Therefore, since the results are not affected to a large degree by Pr, the value Pr =2/3 is used for our subsequent calculations.

Table 6-1 Comparison between solution of energy equation under laminar flow condition for values of Pr =2/3 and 0.707 for $M_0 = 0.8$, $\xi_\infty = 200$ and number of nodes = 20,000.

	Pr = 2/3	Pr =0.707(Air)	
ξ	Θ	Θ	% Difference
0	0.9330	0.9289	0.43
0.5	0.9334	0.9294	0.43
1	0.9452	0.9418	0.35
1.5	0.9663	0.9643	0.21
2	0.9795	0.9783	0.13
2.5	0.9866	0.9858	0.08
3	0.9906	0.9900	0.06
3.5	0.9931	0.9926	0.04
4	0.9947	0.9944	0.03
4.5	0.9958	0.9955	0.03
5	0.9966	0.9964	0.02

Table 6-2 Comparison between solution of energy equation under laminar flow for Pr =2/3 and 0.716, for $M_0 = 0.8$, $\xi_\infty = 200$ and number of nodes = 20,000.

	Pr = 2/3	Pr =0.716	
ξ	Θ	Θ	% Difference
0	0.9330	0.9280	0.53
0.5	0.9334	0.9285	0.53
1	0.9452	0.9411	0.43
1.5	0.9663	0.9638	0.26
2	0.9795	0.9780	0.15
2.5	0.9866	0.9856	0.10
3	0.9906	0.9899	0.07
3.5	0.9931	0.9926	0.05
4	0.9947	0.9943	0.04
4.5	0.9958	0.9955	0.03
5	0.9966	0.9963	0.03

6.3 Effect of Mach number on Temperature, Density and Pressure

The radial momentum equation (3.1.10) implies that the centrifugal force is balanced by the rate of change of pressure in the radial direction, which is directly proportional to the radius. Therefore, increase in the centrifugal force will cause a corresponding increase in the static pressure see Figure 6.1.

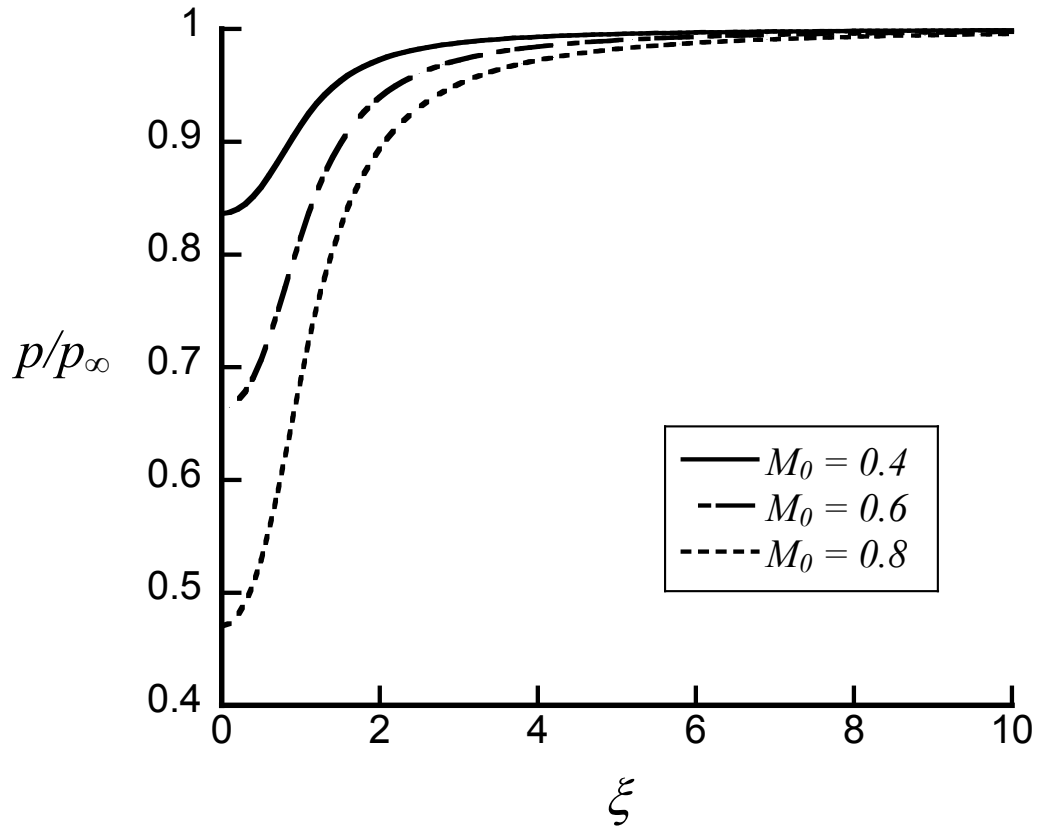

Figure 6.1 Variation of dimensionless pressure vs. vortex Mach number for a laminar vortex for Pr=2/3, number of nodes =20,000, $\xi_\infty = 200$. (Note that p/p_∞ is equivalent to $\Pi\gamma M_0^2$)

As the fluid element moves from the outer periphery towards the vortex center, the fluid element expands. Consequently, the temperature and density decrease towards the vortex center see Figures 6.2 and 6.3. The drop in the temperature and density at the center become more at higher Mach numbers.

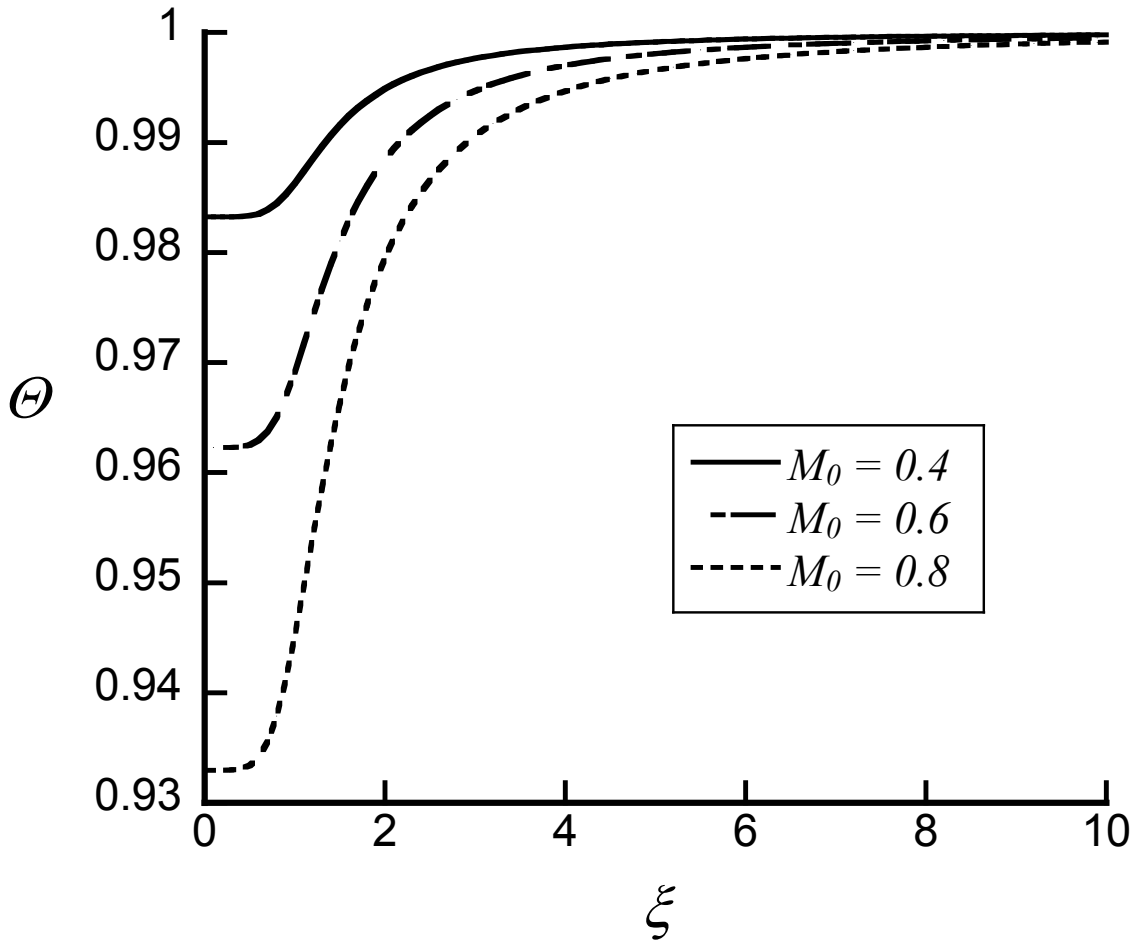

Figure 6.2 Variation of dimensionless temperature vs. vortex Mach number for a laminar vortex with Pr =2/3, ξ_∞ = 200, and number of nodes = 20,000.

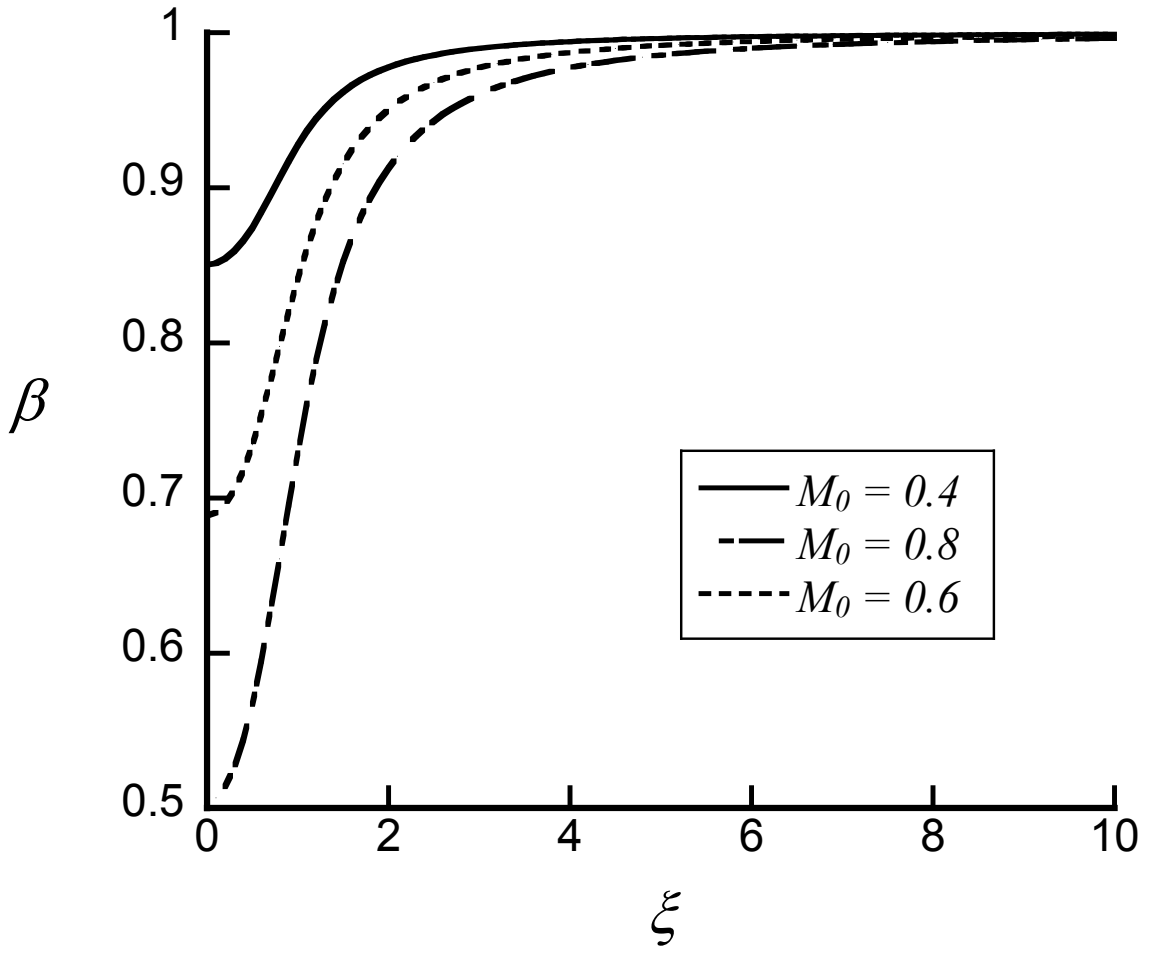

Figure 6.3 Variation of Density vs. vortex Mach number for a laminar vortex with Pr =2/3, ξ_∞ = 200 and number of nodes = 20,000.

6.4 Second Law of Thermodynamics applied to Laminar Compressible Vortex Flow

All governing equations are derived from the conservation equations of mass, momentum, and energy along with the state equation. In order to be realistic the model must also obey the second law of thermodynamics, i.e. entropy must increase in flow direction. The Oswatitsch's (1945) entropy equation, when applied to the laminar compressible vortex under consideration gives,

$$\left(\Delta S\right)_{\xi} = \ln(\Theta)_{\xi} + \left(\gamma - 1\right) M_0^2 \left[\int_0^{\infty} \frac{V^2}{\xi \Theta} d\xi - \int_0^{\xi} \frac{V^2}{\xi \Theta} d\xi \right] \tag{6.4.1}$$

A more detailed description of the above equation is mentioned in Appendix A.

The result shown in Figure 6.4 confirms that our mathematical model does indeed obeying the second law of thermodynamics, namely the entropy increases stream wise. The variation of entropy with different vortex Mach numbers is also shown in the same Figure.

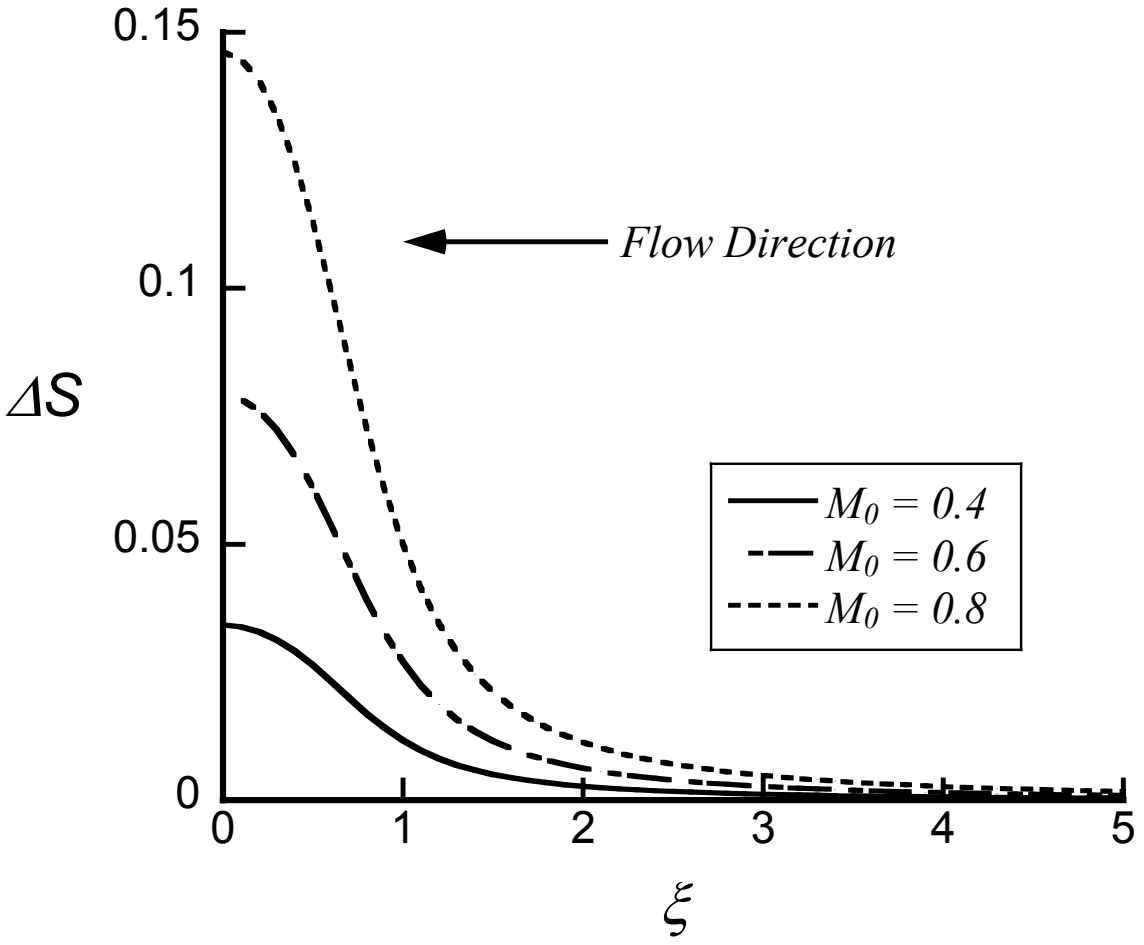

Figure 6.4 Change in Entropy with vortex Mach number for a laminar vortex with Pr =2/3, $\xi_\infty = 200$, and number of nodes = 20,000.

6.5 Explanation of Decrease in Temperature towards Centre of Vortex

The change of temperature as a function of the radius is given by equation (4.1.3) can be expanded as follow:

$$-\frac{d\Theta}{d\xi} = \Pr(\gamma-1)M_0^2 \frac{\int_0^{\xi} f\,\xi\lambda d\xi}{\xi\lambda} + \Pr(\gamma-1)M_0^2 \frac{\int_0^{\xi} UV^2\lambda d\xi}{\xi\lambda} \qquad (6.5.1)$$

$$F = \begin{pmatrix} \text{Heating of Fluid} \\ \text{Element} \\ \text{Due to Friction} \end{pmatrix} \qquad D = \begin{pmatrix} \text{Cooling of Fluid} \\ \text{element} \\ \text{Due to expansion} \end{pmatrix}$$

The negative sign in front of temperature derivative indicates that the fluid element is moving from the periphery towards the vortex center.

The results for a laminar vortex are plotted in Figure 6.5.

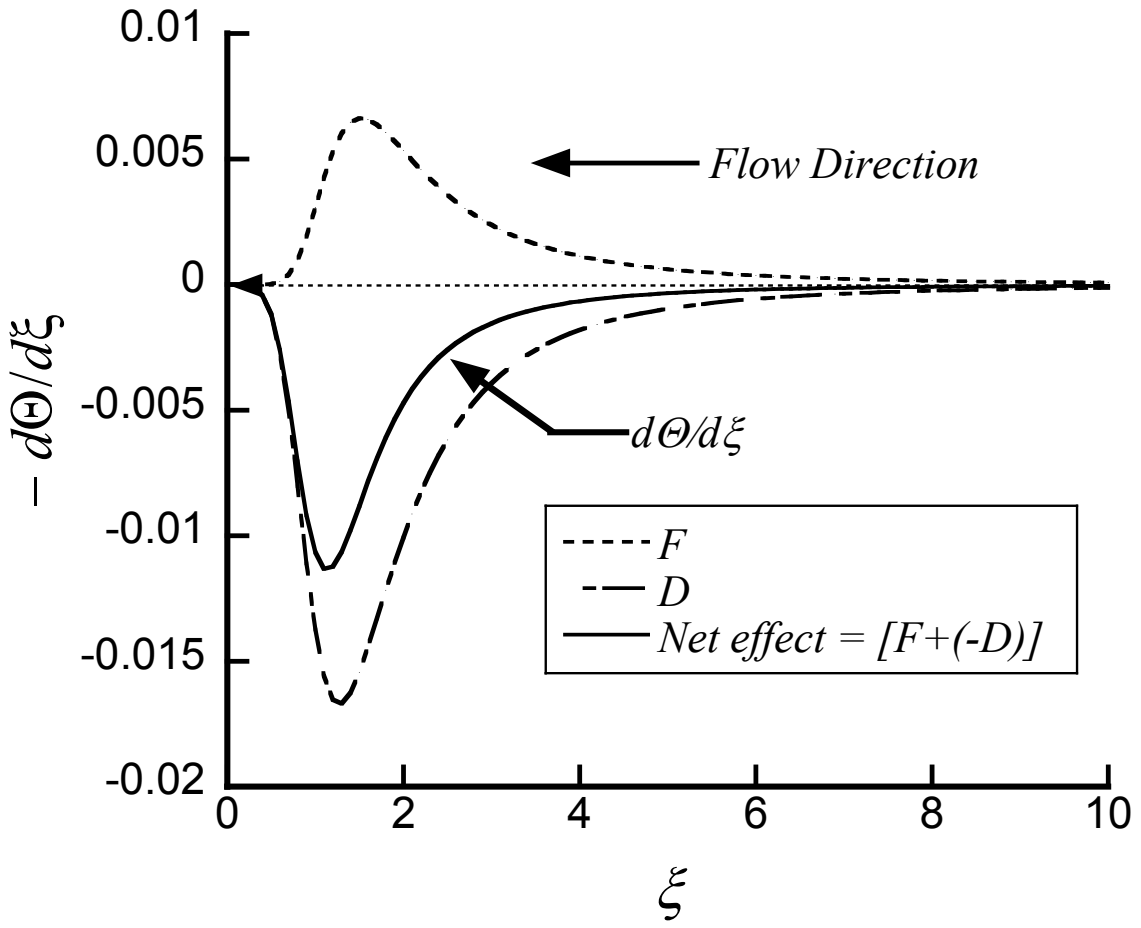

Figure 6.5 Net effect of heating and cooling of fluid element due to viscous dissipation and fluid element expansion respectively in a laminar vortex for M_0=0.4, with Pr =2/3, ξ_∞ = 200, and number of nodes = 20,000.

It is clear from Figure 6.5 that as the fluid element is moving along the flow direction (negative radial direction), it comes under the influence of two effects i.e. heating of fluid element due to viscous forces which ultimately tends to increase its temperature. Pressure is also decreasing (see Figure 6.1) in flow direction. Therefore, the fluid element expands (the volume of the elementary fluid element is proportional to $1/\beta$). This causes cooling of the element.

It is apparent from Figure 6.5 that $\left(F < D\right)$ and D is always negative. Therefore, the net effect of heating of fluid element (F) due to friction and cooling down (D) due to expansion is always negative $\left[\left\{F + (-D)\right\} < 0\right]$ throughout the radial interval [0, ∞). Because of this, the temperature decreases monotonically from ∞ to 0, attaining a minimum at center of the vortex.

Rott (1959) looking for exact solutions to the equations of compressible line vortices came across the static temperature decrease. However, being aware of his model's limitations remarked that the applicability of his results to the Ranque-Hilsch tube is doubtful for several reasons. Most important of them being that the formulation could not predict the 'hot' side of the phenomenon. The "… only modest values of heating" Rott (1959) that he discovered pertains to the stagnation and not to the static temperature. The static temperature (like for a = 1 case) is below the ambient throughout the field. Understandably, the forecast of the "hot" feature was not possible because Burgers's (1948) vortex is not applicable to turbulent vortices. In addition, since the radial velocity in Burgers vortex varies linearly with the radius, the formulation is inappropriate for unconfined vortices. The last is evident from several observations where the radial velocity is far from being directly proportional to the radius see for example Hite and Mih (1996) and Trenberth et al. (2007).

7 Results for Turbulent Compressible Vortex Flow

7.1 Verification of the numerical procedure

Before we proceed with the discussion of results through productive runs it is important that we deal first with some important numerical issues.

Alike to the laminar compressible vortex all the integrals in the energy equation are evaluated numerically via the recursive adaptive Lobatto quadrature, with tolerance error of 10^{-6}. The results have also been verified through the symbolic algebra system *Theorist* (an older version of LiveMath) as well as numerically using a central finite difference solver. Also, the computational turbulent vortex results, for Pr = 2/3, M_0= 0.8, a = 0.7, ξ_∞ = 200, and number of nodes = 20,000, indicated that the residual ε in the energy equation,

$$\frac{d}{d\xi}\left(\xi\frac{d\Theta}{d\xi}\right) - \mathrm{PrU}\xi\frac{d\Theta}{d\xi} + \mathrm{Pr}\left[\gamma - 1\right]M_0^{\,2}\left(f\xi + UV^2\right) = \varepsilon$$

was less than $\pm\, 2\times10^{-8}$. See Figure 7.1.

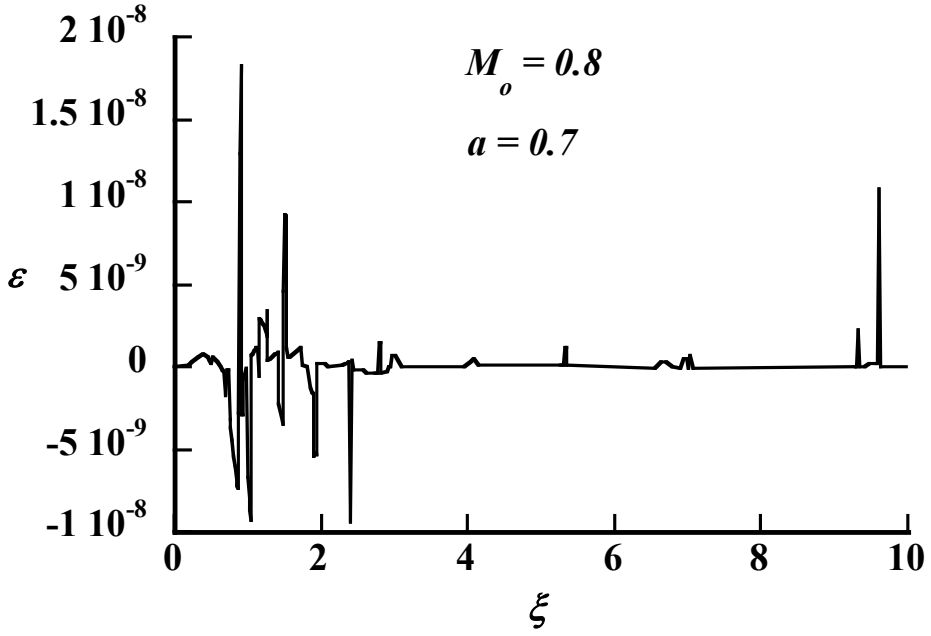

Figure 7.1 Residual of solution of energy equation under turbulent compressible vortex flow condition with Pr=2/3, M_0= 0.8, a = 0.7, ξ_∞ = 200 and number of nodes=20,000.

The integrals in the rate and temperature equation involve infinite limits. The last requires integration until a radius, which is satisfactorily far away from the center of the vortex. Numerical experiments for the temperature $\Theta_{\xi=0}$ with different values of ξ_∞ are shown in Figure 7.2. These indicated that the relative difference between values of $\Theta_{\xi=0}$ when ξ_∞ is taken as 200 and 400 was only 7.2×10^{-4}. Thus, in order to economize on the computations, a radius of ξ_∞ = 200 was finally deemed to be sufficiently "far" without loss of physics. This is the criterion for infinity that we adopted for our computations for both laminar as well as turbulent vortices.

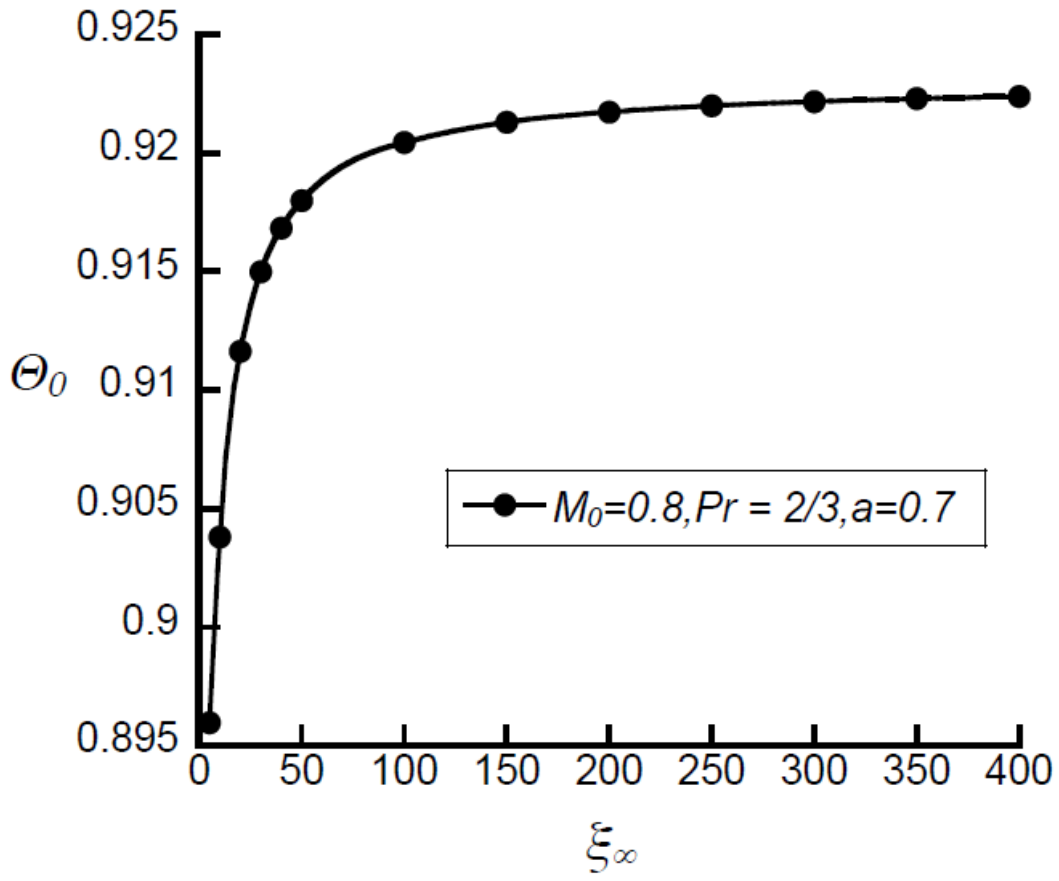

Figure 7.2 Variation of temperature at vortex center vs. ξ_∞ with parameters M_0=0.8, Pr=2/3, number of nodes=20,000 and a=0.7.

The effect of Prandtl number on the results of the energy equation for a turbulent vortex was also examined. The results for M_0 =0.8 and are shown on Tables 7.1 and 7.2. These indicate that the maximum difference occur at $(\xi = 2.0)$ yielding a small percentage difference.

Table 7-1 Comparison between solution of energy equation under turbulent flow condition for values of Pr =2/3 and 0.707 with M_0 =0.8, $\xi_\infty = 200$ and number of nodes=20,000.

	Pr = 2/3	Pr = 0.707	
ξ	Θ	Θ	% Difference
0	0.9217	0.9226	0.10
0.5	0.9228	0.9237	0.10
1	0.9482	0.9504	0.23
1.5	0.9870	0.9904	0.34
2	1.0091	1.0126	0.35
2.5	1.0195	1.0227	0.31
3	1.0241	1.0270	0.28
3.5	1.0260	1.0285	0.24
4	1.0265	1.0287	0.21
4.5	1.0263	1.0282	0.18
5	1.0258	1.0274	0.16

Table 7-2 Comparison between solution of energy equation under turbulent flow condition for values of Pr=2/3 and 0.716 with M_0 =0.8, $\xi_\infty = 200$ and number of nodes=20000.

	Pr = 2/3	Pr = 0.716 (Nitrogen)	
ξ	Θ	Θ	% Difference
0	0.9217	0.9228	0.12
0.5	0.9228	0.9239	0.13
1	0.9482	0.9508	0.28
1.5	0.9870	0.9911	0.41
2	1.0091	1.0133	0.42
2.5	1.0195	1.0233	0.38
3	1.0241	1.0276	0.33
3.5	1.0260	1.0290	0.29
4	1.0265	1.0291	0.25
4.5	1.0263	1.0286	0.22
5	1.0258	1.0277	0.19

Moreover, if someone takes Pr =2/3 for Nitrogen in place of its actual value of 0.716, the maximum percentage difference occurs at $(\xi = 2.0)$ and it is less than 0.5%. Thus, there is insignificant change in the solution of the energy equation with modest changes in the Prandtl number values. Therefore, from now onwards we will assume a Pr =2/3 for rest of the calculations.

Experimental work that deals with the detail profiles of the main fluid dynamic parameters for unconfined vortices is limited. Due to the small size of vortex tubes

reliable experimental radial profiles of any fluid property is also hard to find. Nevertheless, as means to partially authenticate the present theoretical model, the pressure data of Pivirotto (1966) in a larger confinement were used. The experimental records for two Mach numbers (0.51and 0.98) depicted in Figure 6.3 show an acceptable agreement with the calculated pressure profiles.

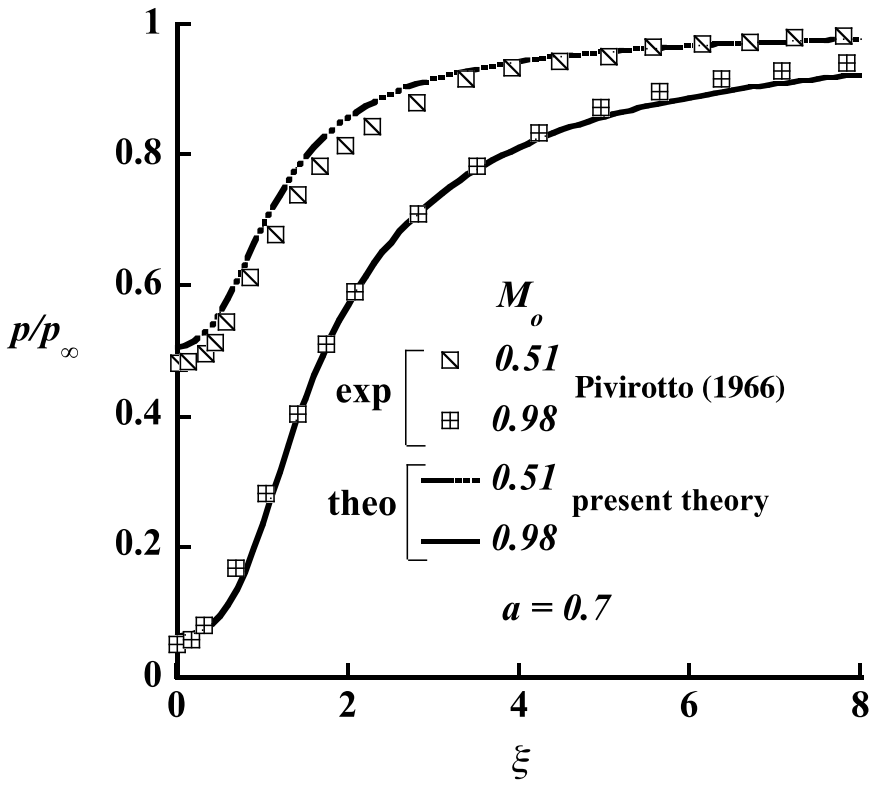

Figure 7.3 Validation of the calculated pressure profiles from Eq.6.1.2, and using the experimental data of Pivirotto (1966). These were performed in a gaseous-vortex reactor (cold), for advanced space propulsion. The comparisons with two datasets (M_0 = 0.51 and 0.98) show a fair agreement between the two. $\xi_\infty = 200$.

Therefore, with all of the abovementioned evidence one can use the present numerical method with sufficient confidence to probe into the very nature of the event.

7.2 Results and discussion of mechanically produced vortices

Equation (4.1.4) is next solved numerically using the expressions of V, f, U, λ for a turbulent vortex. The results of the temperature distribution are given in Fig. 7.4.

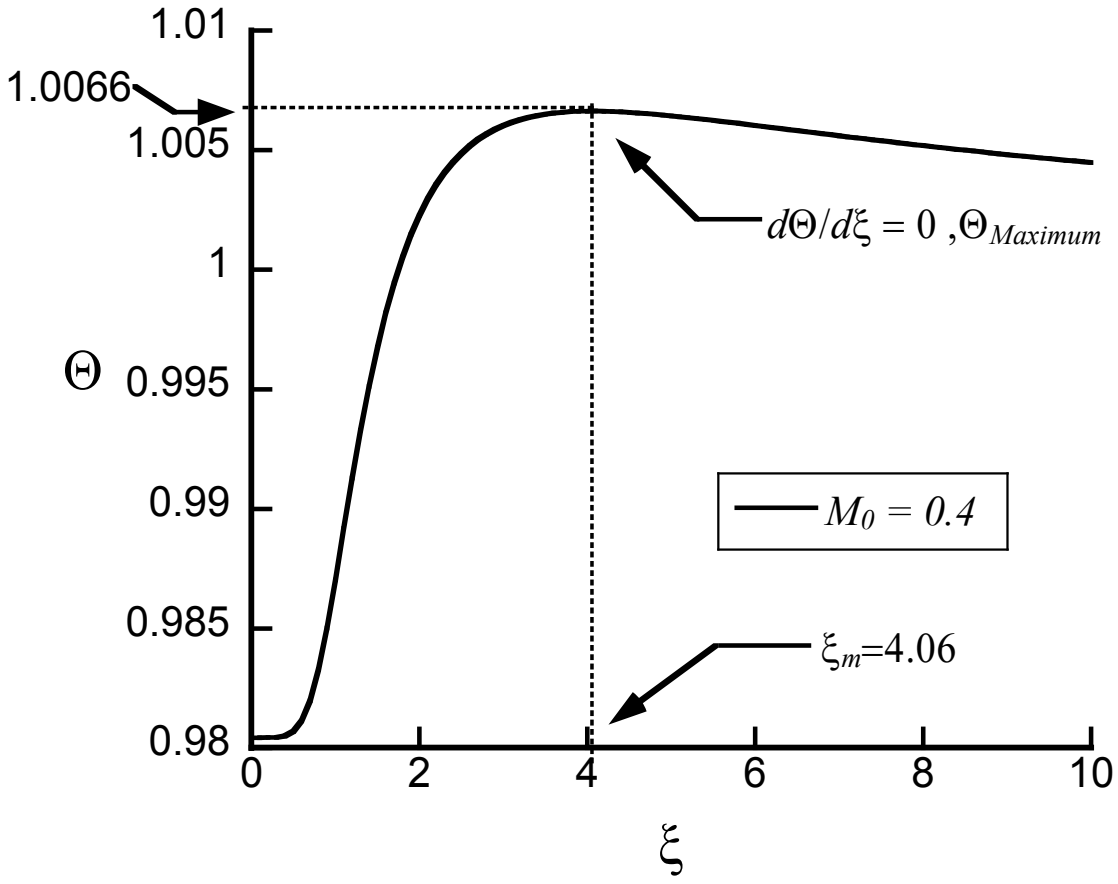

Figure 7.4 Variation of temperature vs. the radius for a = 0.7, Pr =2/3, $\xi_\infty = 200$, M_0 = 0.4 and number of nodes=20,000.

The graph shows that as the fluid element moves from far towards the vortex center increases. It attains a maximum value of temperature at $(\xi_m = 4.06)$, and then it starts to decrease, reaching finally a minimum at the center of the vortex.

In order to explain this phenomenon, one has to pay attention what happens to the fluid element as it moves towards the center. This could be explained using equation (6.5.1).

As shown in Figure 7.5, there is a competition between heating of the element due to viscous action (F) and cooling due to its expansion (D). Viscous dissipation tries to heat up the element. As the fluid moves towards the lower pressure region it expands and hence its temperature decreases. Therefore, the net effect of F and D will decide whether the temperature increases or decreases.

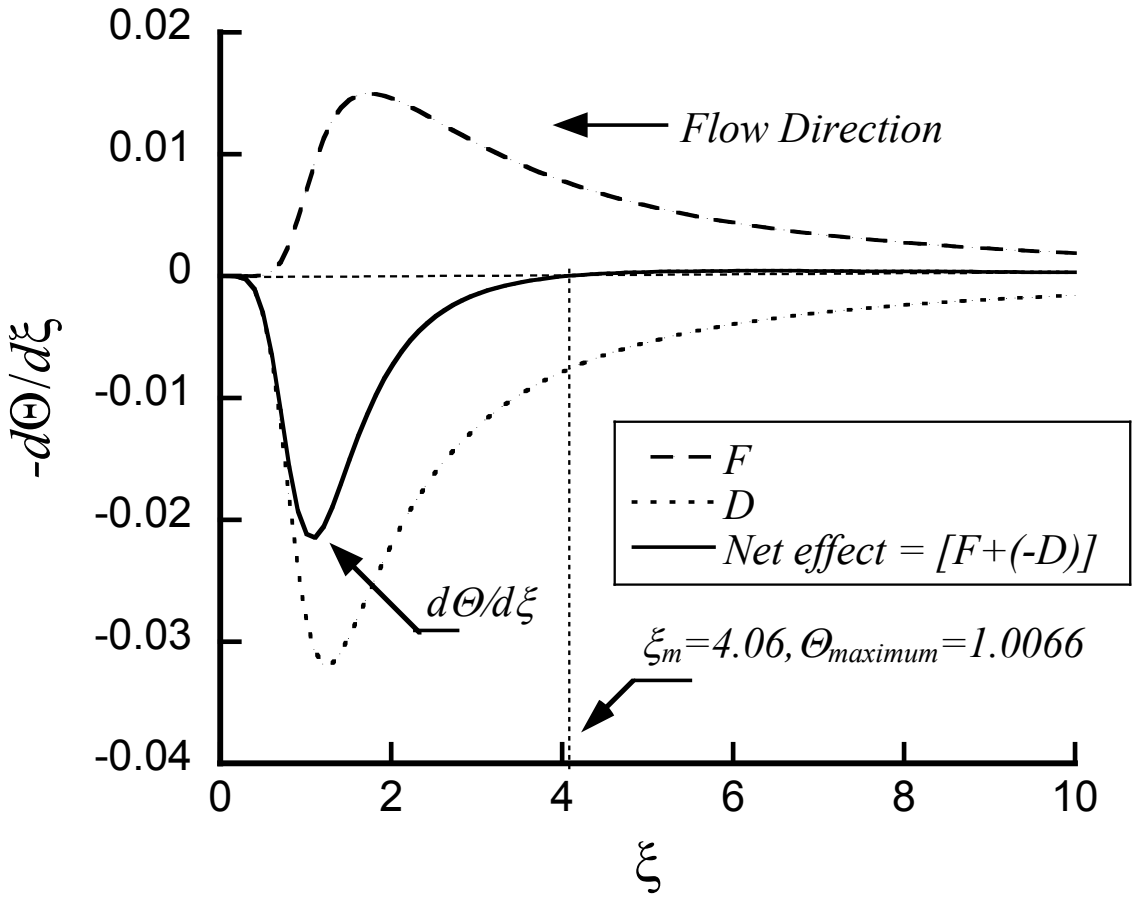

Figure 7.5 Net effect of heating and cooling of fluid element due to viscous dissipation and expansion respectively for a=0.7, Pr=2/3, $\xi_\infty = 200$, $M_0 = 0.4$ and number of nodes=20,000.

In the interval (∞, ξ_m), heating of fluid element due to friction (F) is greater than cooling (D). The combined effect will be positive or the fluid will heat up. At $\xi_m \sim 4.06$, F = D (or the temperature derivative is zero) and hence the temperature will achieve its maximum value$\left(\Theta_{max} = 1.0066\right)$. For radii$\left(0 < \xi < 4.06\right)$, cooling of fluid element (D) due to expansion is more than heating of the fluid element (F) due to friction. The net effect will cool the gas down. The temperature minimum will of course occur at the vortex center, where the derivative of the temperature is zero. The Ranque-Hilsch thermal

effect was discovered in vortex tubes but it is not exclusive to this particular application. The observations of the stream wise isolated vortex within a supersonic stream Cattafesta and Settles (1992) show indeed a similar characteristic for the temperature (see their fig. 7). After more than 80 years from its discovery, the last analysis identifies clearly the mechanism that gives rise to the general Ranque-Hilsch temperature separation.

The effects of Vortex Mach number are shown in Figure 7.6. As the vortex Mach number increases the temperature at the hottest spot goes up and the minimum temperature at the center decreases. However, the radial locations where the temperature maximum occurs and the radius at which Θ crosses the ambient value of one remain the same. Therefore, the degree of temperature separation is a function of the Mach number; the higher M_0 the higher the heating and cooling of the gas.

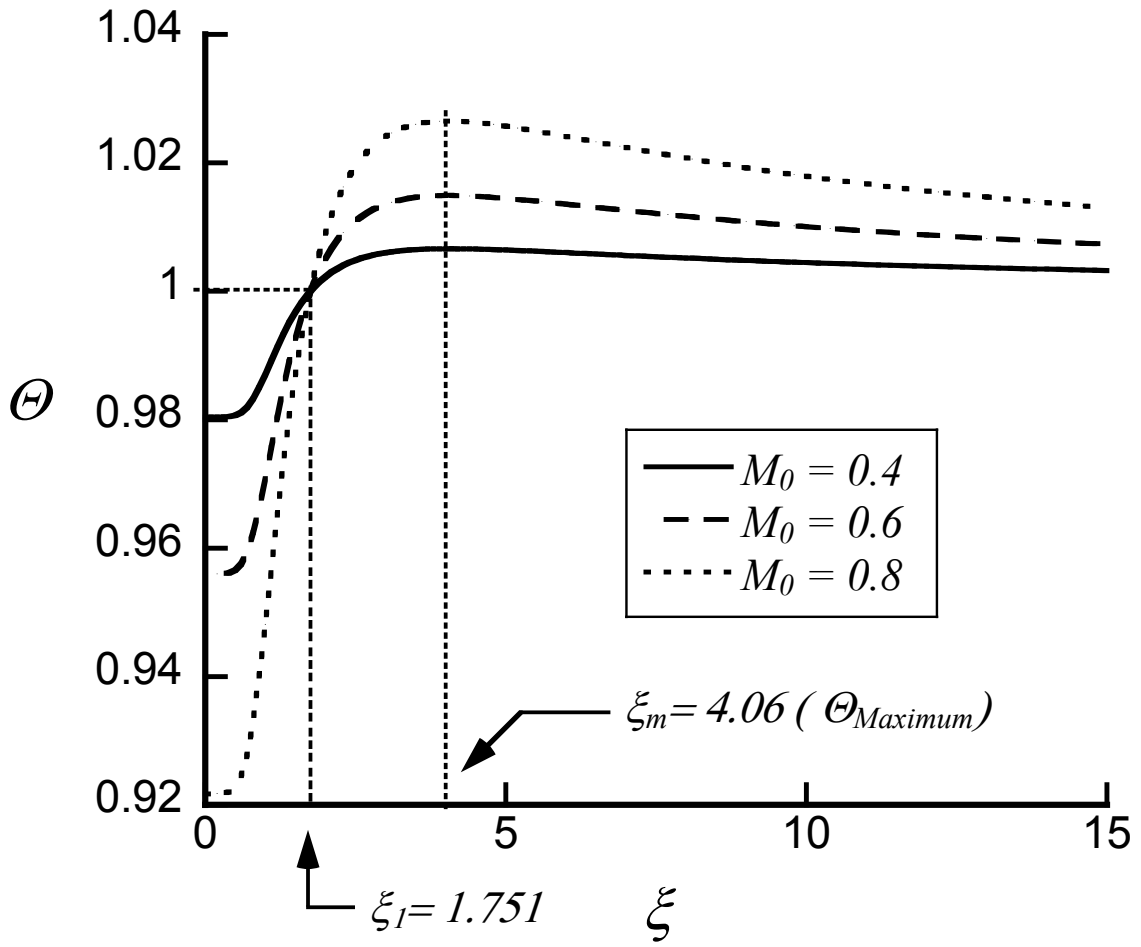

Figure 7.6 Dimensionless temperature vs. vortex Mach number for turbulent vortex for a=0.7, Pr=2/3, $\xi_\infty = 200$ and number of nodes=20,000.

The temperature, density and pressure values for a turbulent vortex are obtained from Eqs. 4.1.4, 6.1.1 and 6.1.2 respectively. These are compared with the corresponding profiles for a laminar vortex. Stream wise, both the pressure and the density decrease monotonically with the radius. Excess friction in a turbulent vortex causes the vortex to attain lower temperature, pressure and density values at the origin. Therefore, excessive friction augments both heating and cooling.

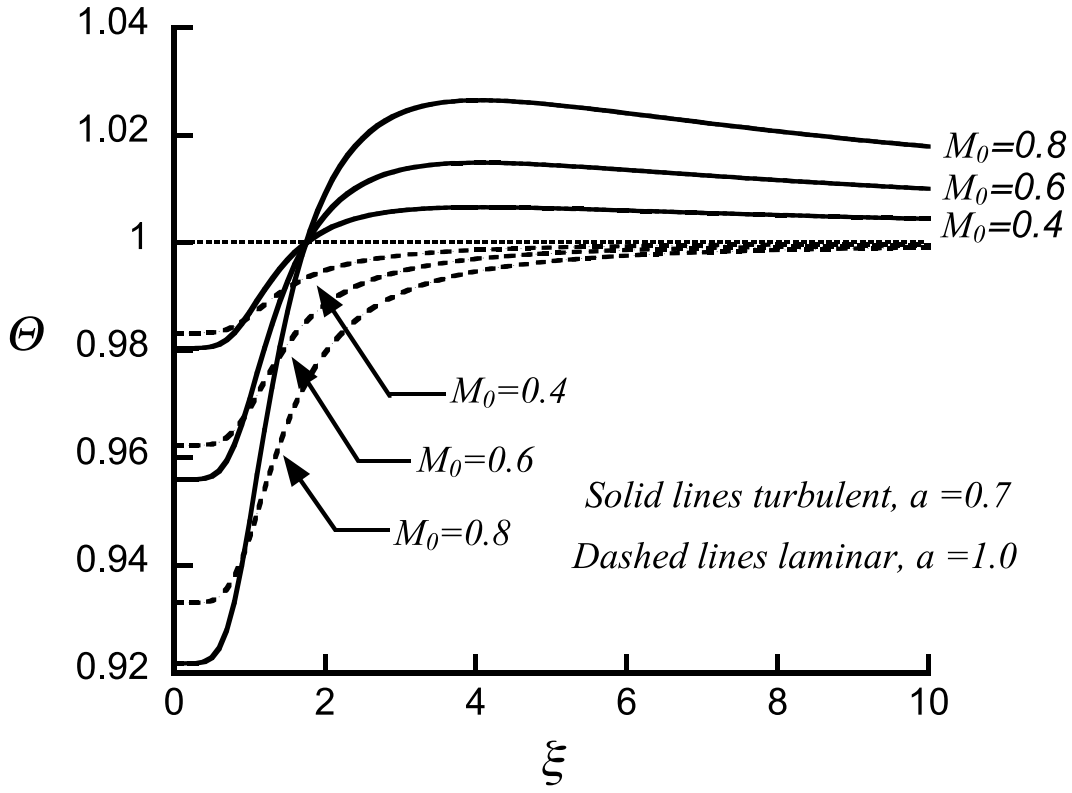

Figure 7.7 Dimensionless temperature variation with vortex Mach number for turbulent vortex for Pr=2/3, $\xi_\infty = 200$ and number of nodes=20,000.

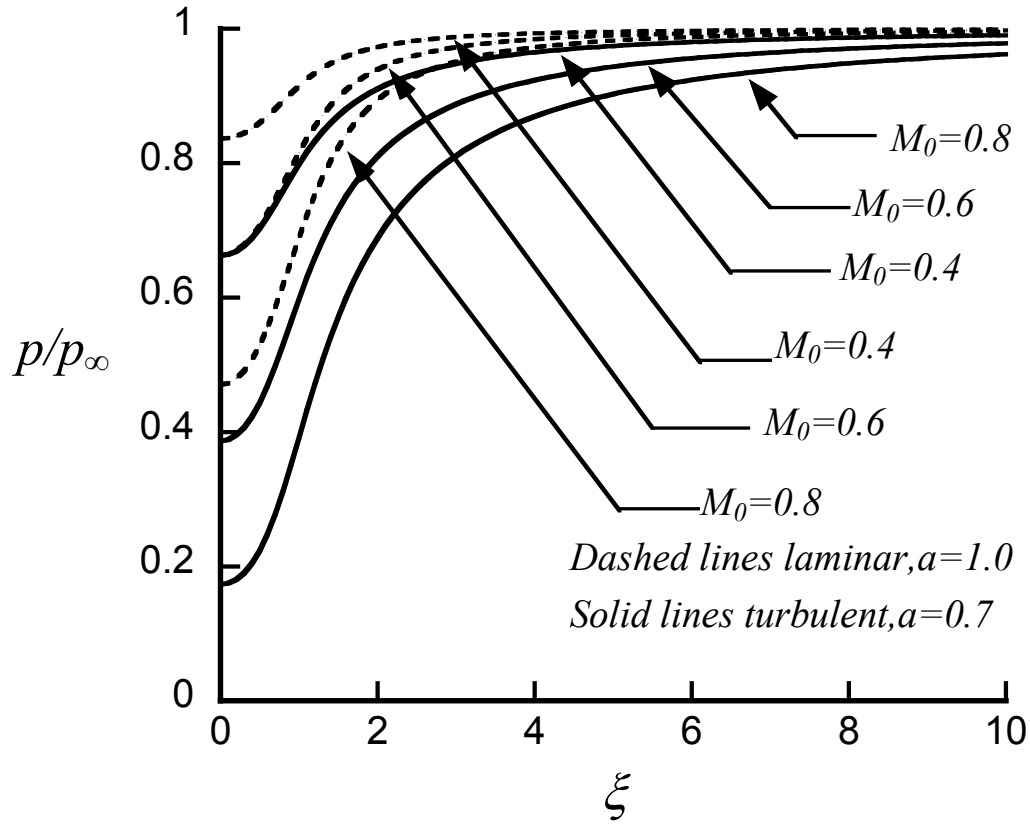

Figure 7.8 Dimensionless pressure variation with vortex Mach number for turbulent vortex for Pr=2/3, $\xi_\infty = 200$ and number of nodes=20,000.

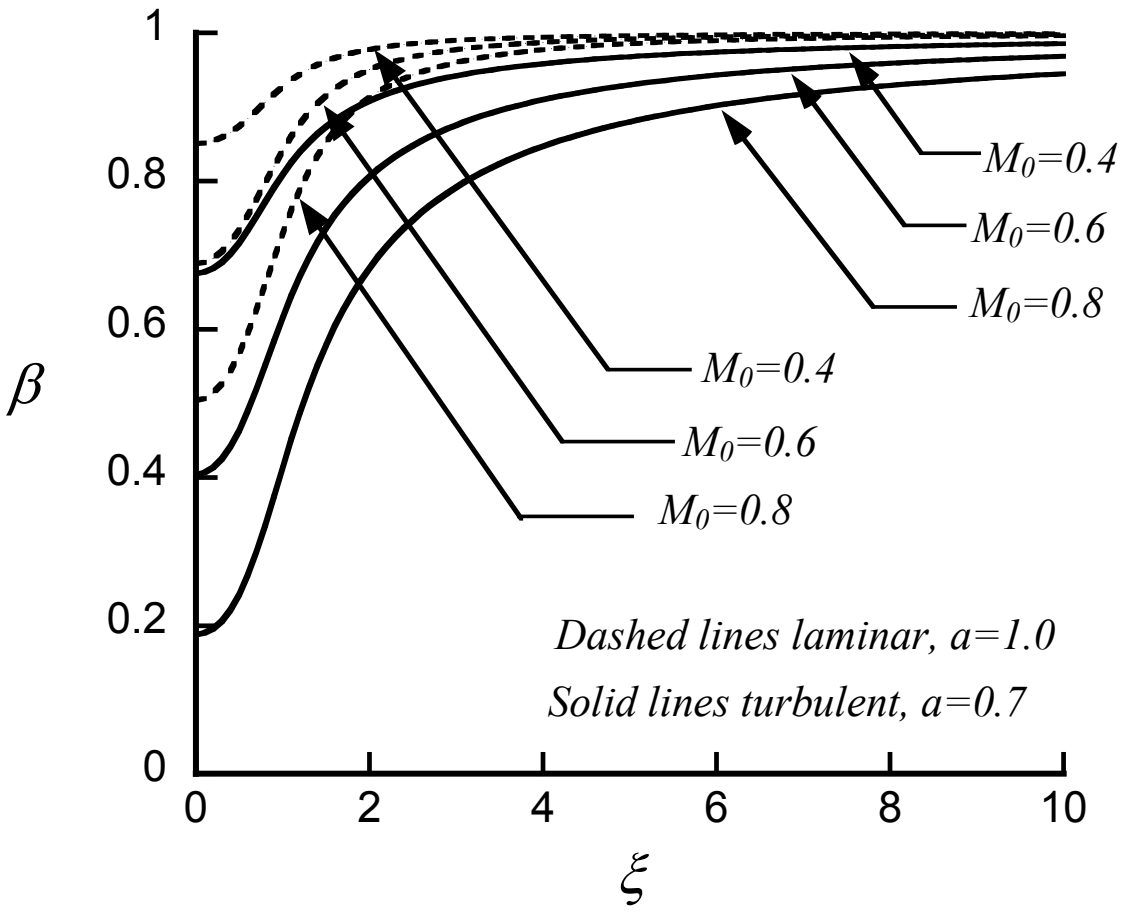

Figure 7.9 Dimensionless density changes vs. vortex Mach number for turbulent vortex for Pr=2/3, $\xi_\infty = 200$ and number of nodes=20,000.

Oswatitsch's (1945) entropy equation given in section (6.4) is applied next to the turbulent flow under the assumptions of intense compressible vortex conditions.

In Figure 7.10, the entropy change is positive $(\Delta S > 0)$ along the flow direction. This demonstrates that the present mathematical formulation for turbulent compressible vortex flow derived in section (3.2) respects also the second law of thermodynamics. The change of entropy obtained from Eq. (6.4.1) for different Mach numbers is shown in the same Figure.

A similar radial profile for the entropy can also be found in the experimental results of Settles and Cattafesta (1993).

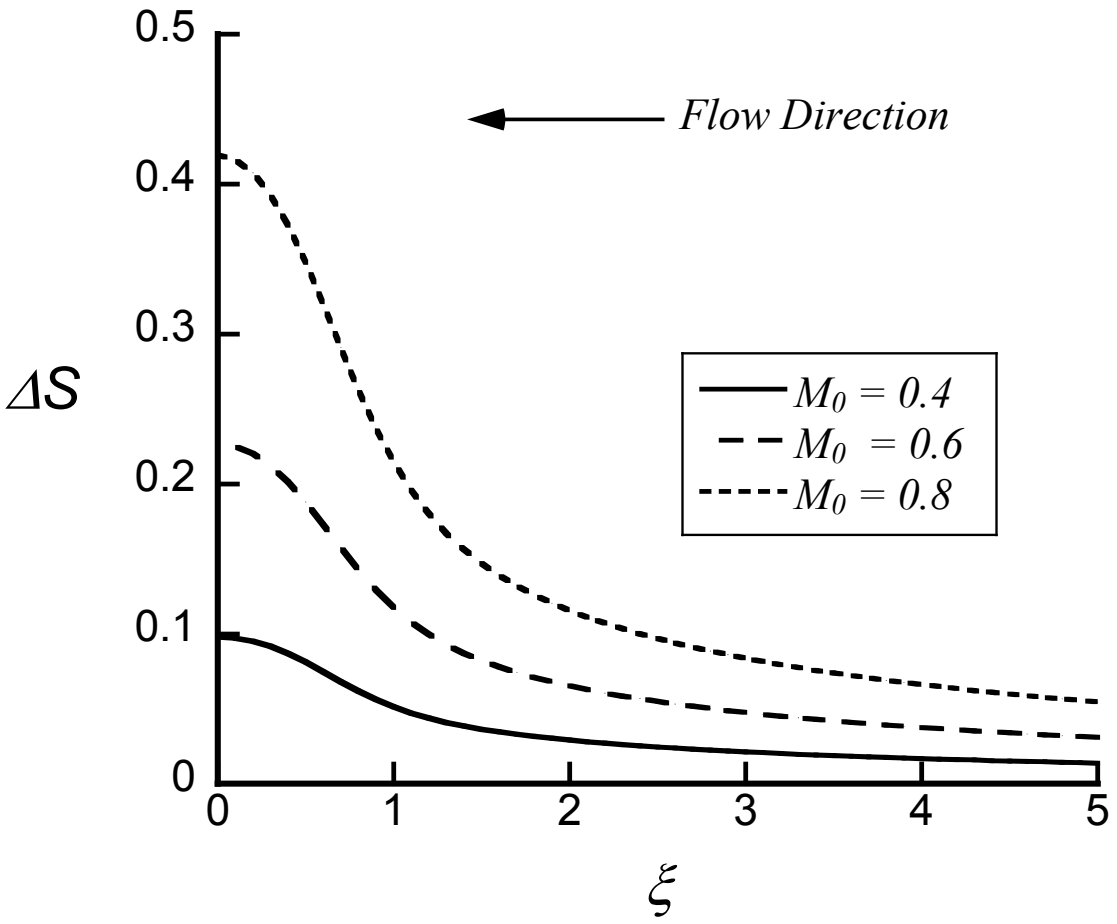

Figure 7.10 Change in Entropy value with vortex Mach number for turbulent vortex for Pr=2/3, a=0.7, $\xi_\infty = 200$ and number of nodes=20,000.

As expected, the change of entropy for laminar flow is less than the turbulent (see Figure 7.11).

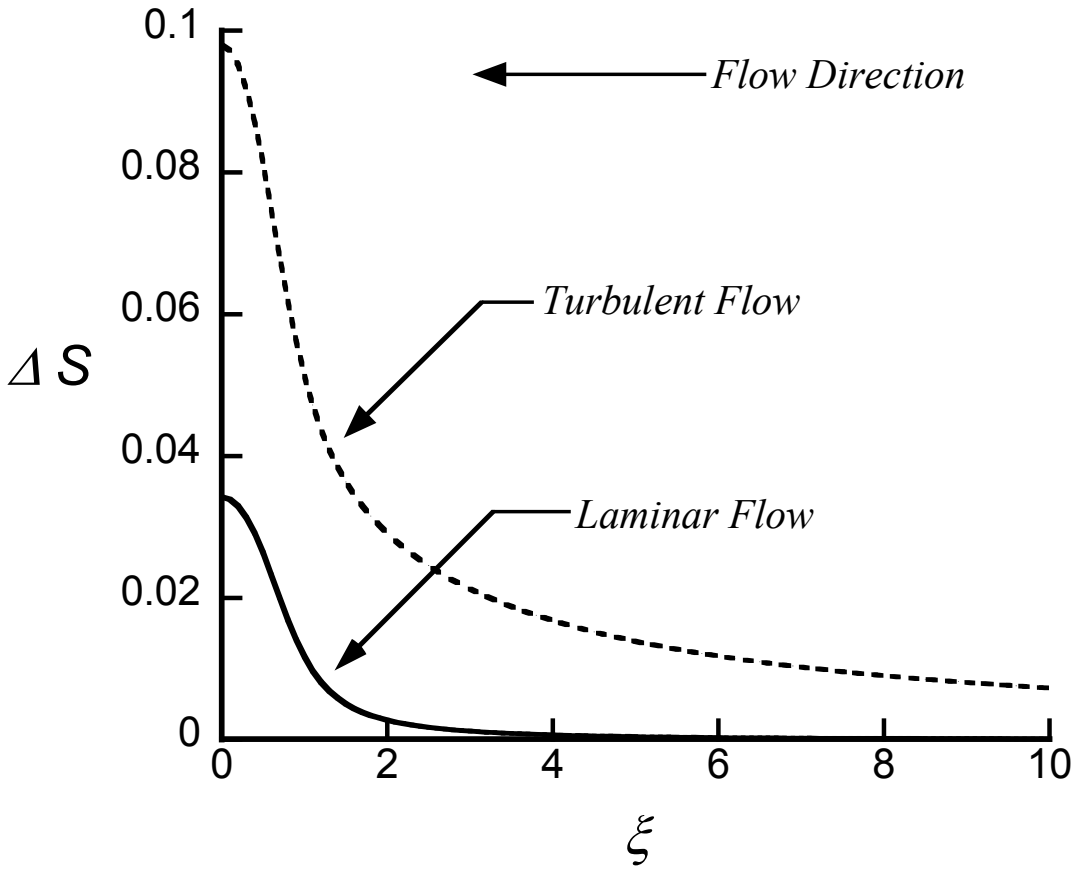

Figure 7.11 Comparison of Change in Entropy of laminar and turbulent compressible vortex for Pr=2/3, $\xi_\infty = 200$ and number of nodes=20,000.

For laminar vortices, constant (a) was equal to one. For present case of turbulent compressible vortex flow, we took a =0.7. This scaling constant (a) represents degree of turbulence. The turbulence levels increase with decreasing of the scaling constant a. It is important to examine the effects that the constant (of turbulence) has on the temperature profile.

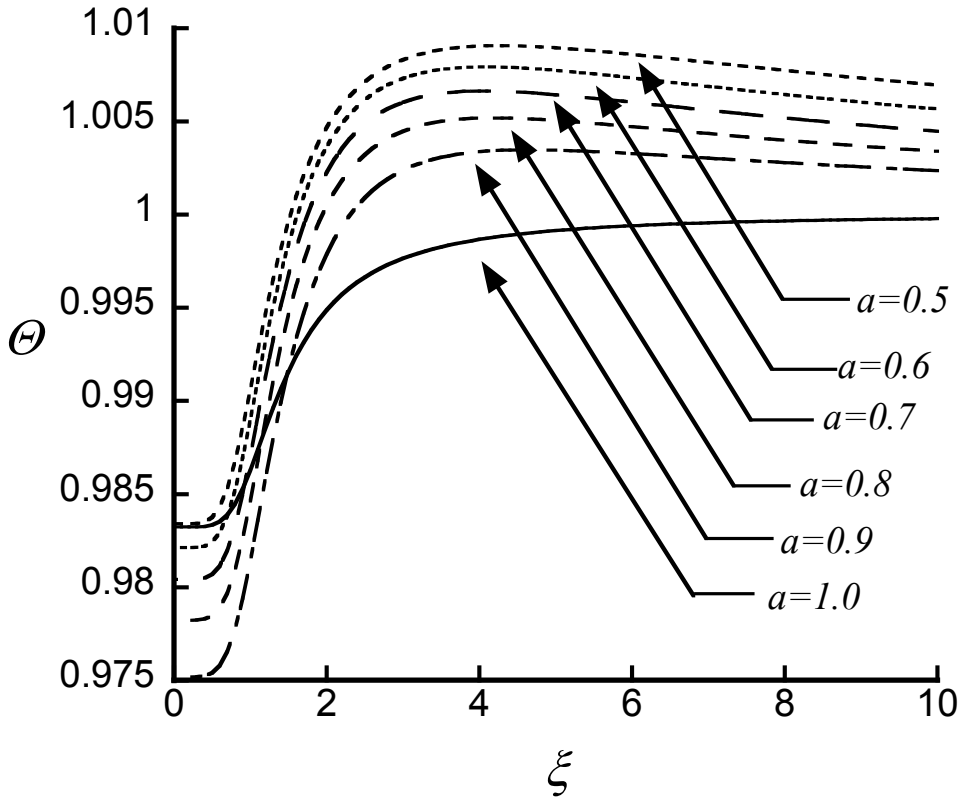

Figure 7.12 Effect of scaling constant (a) on temperature profile of turbulent vortex flow for Pr=2/3, $\xi_\infty = 200$, M_0=0.4 and number of nodes=20,000.

Figure 7.12 shows that the dimensionless temperature for laminar case (a =1.0) has a maximum at ξ_∞. For turbulent flow (a<1) the maximum value of temperature is seen to increase at the maximum radius location and to drop further at the center with parameter a. The last is indeed consistent with the previous statement: "excessive friction augments both heating and cooling". As the degree of turbulence increases the location of Θ_{max} is seen to move towards the vortex center.

8 The Ranque-Hilsch effect in Atmospheric Vortices

The Ranque-Hilsch effect can also be found in in atmospheric vortices such as tornadoes and mature waterspouts. These having a high Rossby number (ratio of inertia to Coriolis force due to Earth's rotation) between 10^3-10^4, bear an intimate similarity to their mechanically produced vortices. Therefore, although intense atmospheric whirls will be used to support the present theoretical results, the conclusions are also applicable to those produced mechanically. In extreme tornadoes and mature waterspouts compressibility effect give rise to Ranque-Hilsch effect. Evidence from these vortices can also be used to validate the present findings.

In chapter 6 and 7, we discussed the two competing mechanisms i.e. heating of fluid element due to viscous forces (F) and cooling (D) due to expansion as it moves towards the lower pressure region. The temperature distribution was plotted in Figure 7.7 that indicated the presence of the Ranque-Hilsch effect.

On June 27 of 1955 a tornado struck Scottsbluff, Nebraska with fury Van Tassel (1955). The estimated tangential velocity for this tornado was found to be 484MPH (215.11 m/s). The vortex Mach number $M_0 = 0.63$ was calculated on the temperature 27 ^0C (80 ^oF) for that day. Figure 8.1 and 8.2 show the results of temperature and density variations for this tornado.

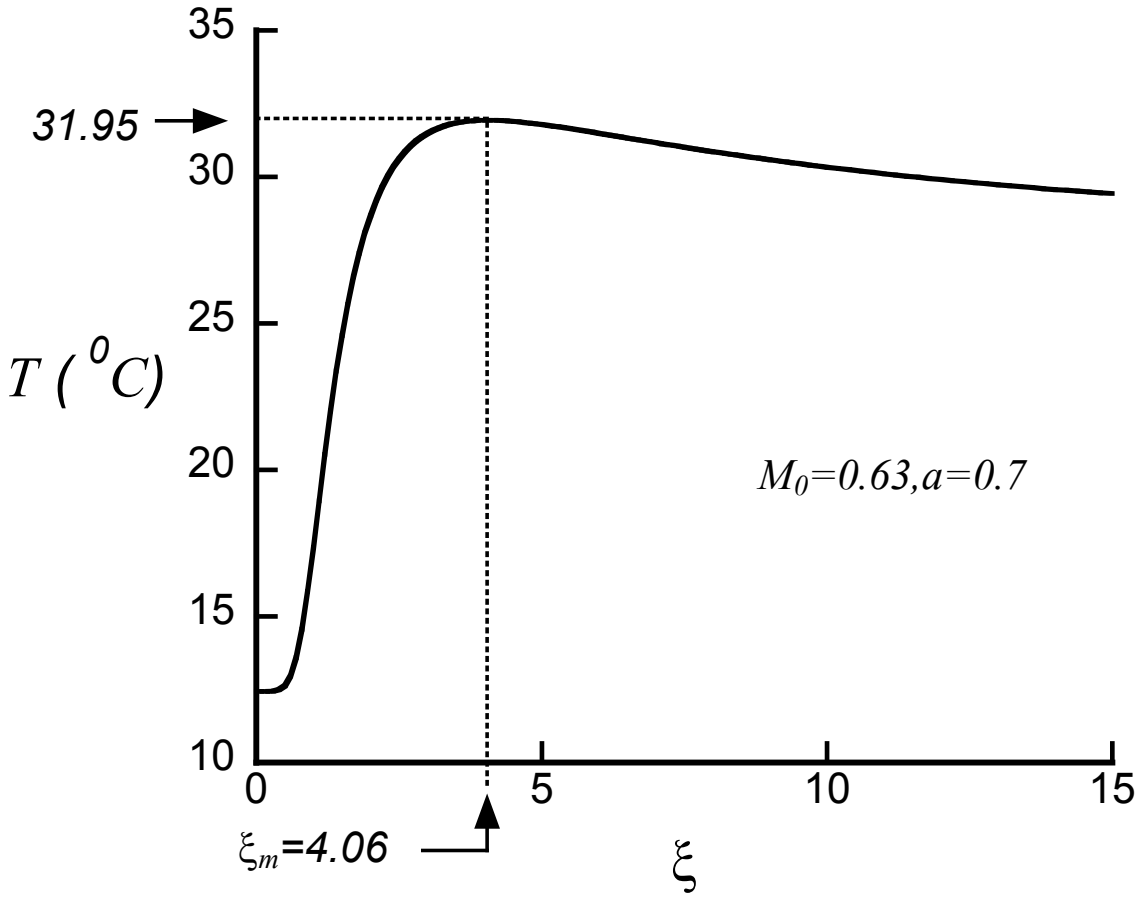

Figure 8.1 Temperature distribution in radial direction in degree Celsius for M_0 =0.63.

Figure 8.1 clearly shows the Ranque-Hilsch effect for the tornado under examination. The hottest region in this tornado is occurring at ($\xi_m = 4.06$) where the temperature reaches 32 ^0C (five degree rise in temperature value than ambient temperature) and minimum temperature at center of vortex equals is 12 ^0C . An observer under the passing Scottsbluff's tornado will feel first a chilling effect due to the sudden drop in temperature of 15 ^0C .

According to Van Tassel (1955) three radio broadcasters reporting this tornado were trapped inside Scottsbluff's cemetery and found shelter in the basement of a

building. During the overhead passage of the tornado they experienced the following odd micro-climatic changes: "… the temperature dropped from a mild summer value until the broadcasters were chilled until they were actually cold." Van Tassel (1955).

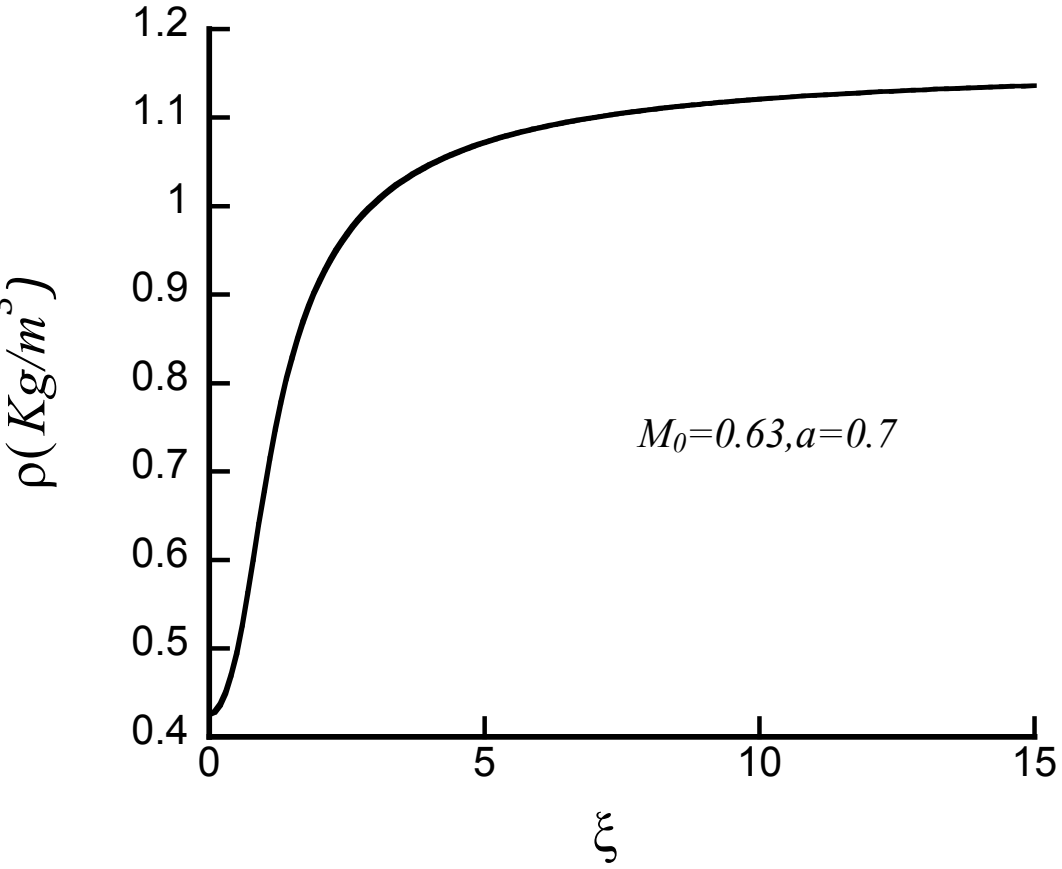

Figure 8.2 Density changes in $\left(\mathrm{Kg/m^3}\right)$ in the radial direction for M_0=0.63.

At center of vortex, the air density from the normal $\rho_\infty = 1.161$ dropped to $\rho_{\xi=0} = 0.4257\ Kg/m^3$. Van Tassel also mentions that the center of the tornado passed about 100 ft. (ξ = 0.9). The density at this distance should be 0.64 Kg/m^3 , which corresponds to the density equivalent to an extreme altitude of about 6,300 m above sea level. Therefore, the oxygen thin conditions made it "difficult to breathe and suffocating"

Van Tassel (1955). Since the tornado had a forward velocity, this physiological effect last for a short period of time.

Furthermore, the radial static pressure distribution, which also includes a substantial deficit at the center of the twister Van Tassel (1955), is alike to the distributions produced by the present model. In fact one of the probes of Lee et al. (2004) registered a pressure deficit of 850 millibars (mb) of Mercury in the 2004 tornado of Manchester, South Dakota. Under their conditions, the present model produced a value of 840 mb. But even the calculated slightly less pressure is justifiable. Their subsequent data analysis indicated that, during this period, the probe was recording events that were taking place certainly inside its funnel but not exactly at the tornado's axis but slightly off center.

Montgomery (see Moore 1955), an observer for U.S Weather Services, recorded the heating effect outside the tornado in Blackwell, Oklahoma (1955). The reported account is: "The air was hot near the funnel, the temperature of my thermometer rises from 74 ^{0}F to 80 ^{0}F when the storm struck".

Another type of atmospheric whirl where the fundamental characteristics of Ranque-Hilsch thermal effect appears is the waterspout. Probes towed from various aircrafts across mature waterspouts produced a number of radial profiles for the temperature. The cumulative results are given in Figure8.3, reproduced from Golden (1974). In his schematic he identified the following temperature anomaly. Moving from the outer periphery towards the center of the waterspout, the static temperature increases, reaching a maximum value, and then dropping to a minimum sub ambient value at the

center of the eddy. Unfortunately, the absence of detailed values for the tangential velocity distribution within these vortices, make a direct comparison of the present analysis with the radial profile of the temperature records weak. Nevertheless, the persistent, from many studies, qualitative heating up, followed by cooling of air reaching the smallest value at the center of rotation, i.e. the Ranque-Hilsch thermal effect, is amply evident.

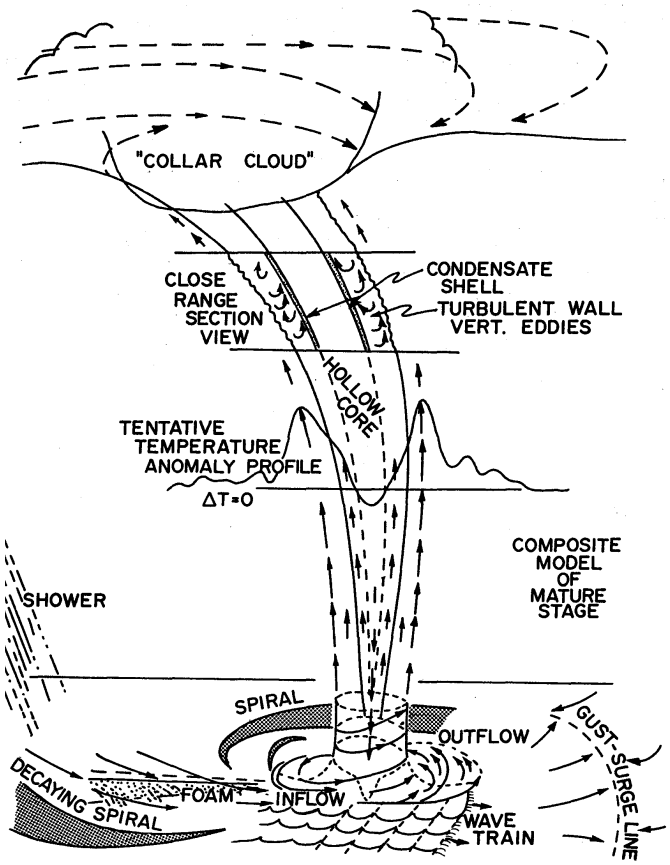

Figure 8.3 The temperature anomaly in mature waterspouts where $\Delta T = T - T_{\infty}$. (From: Golden (1974)).

9 Conclusions

In present study, the laminar compressible vortex flow was extended into turbulent compressible vortex flow by combining the previously proposed tangential velocity model with the proceeding work on the laminar compressible vortex flow. The general form of equations of the conservation of mass, Three Navier –Stokes equations describing the compressible vortex flow were simplified by assuming steady, axis symmetric flow, where body forces acting on the fluid element were neglected. The equations in dimensionless form were further simplified under intense vortex flow condition. The undetermined system of equations was solved assuming a turbulent tangential velocity component and introducing the energy and state equations.

The modified tangential velocity formula (n=2) was used to determine the radial velocity component from tangential-momentum equation, whereas the axial velocity component was deduced using conservation of mass equation. The energy equation was solved for both laminar and turbulent compressible vortex flow conditions for any value of Prandtl Number using numerical integration routine quadl embedded in the Matlab software.

Comparing the results against the exact solution verified the numerical solution of energy equation under laminar flow conditions. The results also suggested that Prandtl number has no significant effect on solution of energy equation. Therefore, one can use the exact solution of energy equation to find the density and pressure distribution using radial-momentum and equation of state respectively. The temperature, pressure and density of a fluid element decreases as it moves towards center.

The results revealed that for laminar flow, cooling of fluid element due to its expansion is always bigger than its heating caused by viscous dissipation. This causes a continuous drop in temperature, attaining minimum value at vortex center. The increased value of vortex Mach number augmented the temperature, density and pressure decrease.

For the case of turbulent compressible vortex, Prandtl number was also found to have an insignificant effect on the energy equation. The radial distribution of density and pressure were calculated using radial-momentum and equation of state respectively. The results of energy equation under turbulent flow condition shows that the temperature of fluid element increases and attaining higher value than ambient from far infinity to certain location of radius. From this location to vortex center, the temperature starts decreasing. In the interval (∞, ξ_m), heating of fluid element due to friction is greater than cooling (D). For radii $\left(0 < \xi < \xi_m\right)$, cooling of fluid element due to expansion is more than heating of the fluid element due to friction. The location of maximum temperature value does not change with vortex Mach number for same value of scaling constant. Both laminar and turbulent mathematical models are obeying the second law of thermodynamics.

The results also reveal that the puzzling Ranque-Hilsch effect represents general thermal phenomenon is akin to all compressible intense vortices. The combined effect of mechanical friction and gas expansion produces the temperature separation into hot and cold regions. The observations made by live witnesses or instruments while inside F5 and F4 tornadoes were found to be in agreement with the present theoretical finding.

10 Future Work

In the present analysis of laminar and turbulent compressible vortex flow, all fluid properties were assumed to be constant with temperature. In reality however, the fluid properties (C_p, Cv, γ ,k and Pr) vary with temperature. Figure 7.7 of section 7.2 indicates that as the Mach number increases the temperature separation enlarges. As the flow becomes supersonic, there are significant changes in temperature values and thus its effect on the fluid properties cannot be neglected.

Therefore, one should formulate a new mathematical model where the fluid properties are functions of temperature. The generalized energy equation, along with the rest relevant conservation equations can then be solved numerically. Since the tangential velocity is known not to depend on compressibility both laminar and turbulent models can be used as a parameter that closes the system of equations. Using this approach one can then explore the physics of supersonic vortices.

References

Aboelkassem,Y. and Vatistas, G.H. (2007) "New Model for Compressible Vortices." *J. Fluid Eng.*, vol.29, no.8, pp.1073-1079.

Burgers, J. M. (1948) "A Mathematical Model Illustrating the Theory of Turbulence." *Adv. Appl. Mech.,* vol.1, pp. 171–199.

Cattafesta, L.N. and Settles, G. S. (1992) "Experiments on Shock/Vortex Interaction." AIAA, paper 92-0315.

Deissler, R. G. and Perlmutter, M. (1960) "Analysis of the Flow and Energy Separation in a Turbulent Vortex." *Int. J. Heat Mass Transfer*, vol.1, pp.173-191.

Golden, J. H. (1974) "The Life Cycle of Florida Keys' Waterspouts. I." *J. Appl. Meteor.,* vol.13, pp. 676-692. Also in Golden, J. H. 1974 "Life Cycle of Florida Keys' Waterspouts." NOAA Technical Memorandum, ERL NSSL-10.

Han, Y. Q., Leishman, J. G. and Coyone, A. J.(1997) "Measurements of the Velocity and Turbulence Structure of a Rotor Tip Vortex." *AIAA J.,* vol.35, no.3, pp. 477- 485.

Helmholtz, H. (1858)"Uber die Integrale der Hydrodynamischen Gleichungen, Welche den Wirbelbewegungen Entsprechen." *J. Reine Angew. Math.,* vol. 55, pp. 25-55.

Hilsch, R. (1947) "The Use of Expansion of Gases in a Centrifugal Field as Cooling Process." *Rev, Sci. Instrum.*, vol.18, no. 2, pp.108-113.

Hite, E.J. and Mih, W.C. (1994) "Velocity of Vertical Vortices at Hydraulic Intakes." *J. Hydraulic Eng*., vol. 120, no. 3, pp. 284-297.

Kalhoran, I. M. and Smart, M. K. (2000) "Aspects of Shock Wave-Induced Vortex Breakdown." *Prog. Aeroep. Sci.*, vol.36, pp.63-95.

Katz, R. (1960) "The Vortex Tube the Tornado." *Geofisica Pura E. Applicata, Milano III*, vol.47, pp. 191-194.

Koval, P.V. and Michaelov, P. S. (1972) “Velocity and Pressure Distributions of Liquid in a Swirl Chamber.” *Teploenergetica*, vol.19, no.2, pp. 25-28.

Lee, J. J., Samaras, T. M. and Young, C. R. (2004) “Pressure Measurements at the Ground in an F-4 Tornado.” 22nd Conf. on Severe Local Storms, Hyannis, MA, Amer. Meteor.

Liew, R., Zeegers, J. C. H., Kuerten, J. G. M. and Michalek, W. R. (2012) “Maxwell’s Demon in the Ranque-Hilsch Vortex Tube.” P*hys. Rev. Lett.*, vol.109, no.5, 054503.

Mack, L. M. (1960) “The Compressible Viscous Heat-Conducting Vortex,” *J. Fluid Mech*., vol. 8, pp. 284–292.

Moore, C. (1955) “Some Observations on the Tornado at Blackwell, Oklahoma 25 May 1955”, Reported by Floyd C. Montgomery, *Weatherwise*, vol.9,no.3, pp. 97-101.

Oswatitsch, K. (1945) “Der Luftwiderstand als Integral des Entropiestromes.” *Nachr. Ges. Wiss. Gottingen. Math.-Phys. Klasse.*, pp. 88-90.

Grasso, F., Pirozzoli, S. and Gatski, R. B. (1999) “Analysis and simulation of a turbulent, compressible starting vortex.” *Phys. Fluids* ,vol.11, no.6, pp. 356-267, doi: 10.1063/1.869885.

Grasso, F. and Pirozzoli, S. (1999) “Asymptotic scaling of a decaying turbulent compressible vortex.” *Phys. Fluids,* vol.11, no.6, pp. 1636-1649, doi: 10.1063/1.870024.

Pivirotto, T. J. (1966) “An Experimental and Analytical Investigation of Concentration Ratio Distributions in a Binary Compressible Vortex Flow.” Jet Propulsion Laboratory Tech. report no. 32-80, California Institute of Technology, Pasadena California.

Rankine, W. J. M. (1858), *Manual of Applied Mechanics,* C. Griffen Co., London, England.

Rott, N. (1959) “On the Viscous Core of a Line Vortex II,” *Zeitschrift fur Angewandte Mathematik und Physik*, vol.10, no.1, pp. 73-81.

Ramasamy,M., and Leishman, J. G. (2006) "A Generalized Model for Transitional Blade Tip Vortices." *Journal of the American Helicopter Society*, vol.51, no.1, pp. 92-103.

Ranque, G. J. (1933) "Experiments on Expansion in a Vortex with Simultaneous Exhaust of Hot air and Cold air." L*e Journal de Physique et Le Radium*, vol.4, no.7, pp.112-115.

Scully, M.P. (1975) "Computation of Helicopter Rotor Wake Geometry and its Influence on Rotor Harmonic Airloads." Aeroelastic and Structures Research Laboratory, Massachusetts Institute of Technology, Cambridge, MA, ASRL TR 178-1.

Settles, G. S. and Cattafesta, L. (1993) "Supersonic Shock Wave/Vortex Interaction." Technical Report on NASA Grant NAG-2-575, Penn State Gas Dynamics Laboratory, Department of Mechanical Engineering, Penn State University.

Sibulking, M. (1962) "Unsteady, Viscous, Circular Flow Part 3: Application to the Ranque-Hilsh Vortex Tube," *J. Fluid Mech*., vol.12, pp. 289-298.

Sullivan, R. D.(1959) "A Two-Cell Vortex Solution of the Navier-Stokes Equations." *J. Aerosp. Sci.,* vol.26, no.11, pp. 767-768.

Taylor, G. I. (1930) "Recent Work on the Flow of Compressible Fluids." *J. Lond. Math. Soc.*, vol.5, pp. 224-240.

Trenberth, K. E., Davis, C. A. and John Fasullo, J. (2007) "Water and Energy Budgets of Hurricanes: Case studies of Ivan and Katrina." J. *Geohys. Res*, 112, D23106.

Van Tassel, E.L. (1955) "The North Platte Valley tornado outbreak of June 27, 1955." *Mon. Weather Rev.*, vol.83, pp.255-264.

Vatistas, G.H., Kozel, V. and Mih, W. C. (1991) "A Simpler Model for Concentrated Vortices.". *Exp. Fluids*, vol.11, no.1, pp.73-76.

Vatistas, G.H., Lin S. and Kwok, C.K. (1986) "Theoretical and Experimental Studies on Vortex Chamber Flows." AIAA J, vol.24, pp. 635-642.

Vatistas, G. H. (1998) "New Model for Intense Self-Similar Vortices." *JPP*, vol.14, no.4, pp. 462–469.

Vatistas, G. H., and Aboelkassem, Y. (2005) “Time Decay of n Family of Vortices.” *AIAA J.*, vol.43, no.6, pp. 1389-1391.

Vatistas, G. H. (2006) “Simple Model for Turbulent Tip Vortices. “ *J. Aircraft*, vol.43, no.5, pp. 1577-1579.

Appendix A

(i) Exact solution of energy equation under laminar flow for a Pr = 2/3.

The exact solution of the energy equation under laminar compressible vortex flow condition is determined analytically by assuming a Pr = 2/3 as follow:

The energy equation is given by (3.1.12),

$$\frac{1}{\xi}\frac{d}{d\xi}\left[\xi\frac{d\Theta}{d\xi}\right] - PrU\frac{d\Theta}{d\xi} = -Pr(\gamma - 1)M_0^2\left[f + \frac{UV^2}{\xi}\right] \quad (1)$$

Multiplying ξ on both sides of above equation gives,

$$\frac{d^2\Theta}{d\xi^2} + \left[\frac{1}{\xi} - PrU\right]\frac{d\Theta}{d\xi} = -Pr(\gamma - 1)M_0^2\left[f + \frac{UV^2}{\xi}\right] \quad (2)$$

The radial and tangential velocity components under laminar compressible vortex flow condition are given as follow:

$$U = \frac{-6\xi^3}{1+\xi^4}, V = \frac{\xi}{\sqrt{1+\xi^4}}$$

The Viscous dissipation function (f) is calculated using tangential velocity component,

$$f = \xi^2\left\{\frac{d}{d\xi}\left(\frac{V}{\xi}\right)\right\}^2 = \frac{4\xi^8}{\left(1+\xi^4\right)^3}$$

Putting $Y = \frac{d\Theta}{d\xi}$, $Y' = \frac{d^2\Theta}{d\xi^2}$, Pr=2/3, $U = \frac{-6\xi^3}{1+\xi^4}$, $V = \frac{\xi}{\sqrt{1+\xi^4}}$ and $f = \frac{4\xi^8}{\left(1+\xi^4\right)^3}$ in equation (2) yields,

$$Y' + \left[\frac{1+5\xi^4}{\xi+\xi^5}\right]Y = \frac{4}{3}(\gamma-1)M_0^2\frac{\left(\xi^8+3\xi^4\right)}{\left(1+\xi^4\right)^3} \tag{3}$$

Let (λ) be the integration factor of above differential equation and is given by,

$$\lambda = e^{\int\left[\frac{1+5\xi^4}{\xi+\xi^5}\right]d\xi}$$

$$\lambda = \xi + \xi^5$$

Multiplying (λ) on both sides of equation (3) and after some straightforward mathematical manipulations yields,

$$Y'\left(\xi+\xi^5\right) + \left(1+5\xi^4\right)Y = \frac{4}{3}(\gamma-1)M_0^2\frac{\xi^5\left(3+\xi^4\right)}{\left(1+\xi^4\right)^2}$$

The first two terms of above equation can be combined together and is written as follow,

$$d\left[Y\left(\xi+\xi^5\right)\right] = \frac{4}{3}(\gamma-1)M_0^2\frac{\xi^5\left(3+\xi^4\right)}{\left(1+\xi^4\right)^2}d\xi \tag{4}$$

Integration of above equation yields,

$$Y\left(\xi+\xi^5\right)=\frac{4}{3}\left(\gamma\text{-}1\right)M_0^2\left[\int\frac{3\xi^5}{\left(1+\xi^4\right)^2}d\xi+\int\frac{\xi^9}{\left(1+\xi^4\right)^2}d\xi\right]$$

Upon solving the integrals of above gives,

$$Y\left(\xi+\xi^5\right)=\frac{4}{3}\left(\gamma\text{-}1\right)M_0^2\left[\left\{\frac{3}{4}\tan^{\text{-}}\left(\xi^2\right)\text{-}\frac{3}{4}\left(\frac{\xi^2}{1+\xi^4}\right)\right\}+\left\{\frac{\xi^2}{2}\text{-}\frac{3}{4}\tan^{\text{-}}\left(\xi^2\right)+\frac{1}{4}\left(\frac{\xi^2}{1+\xi^4}\right)\right\}\right]+C_1$$

Where C_1 is the constant of integration and further simplifications of above equation yields,

$$Y=\frac{2}{3}\left(\gamma\text{-}1\right)M_0^2\left[\frac{\xi^5}{\left(1+\xi^4\right)^2}\right]+\frac{C_1}{\left(\xi+\xi^5\right)} \tag{5}$$

Inserting back $Y=\frac{d\Theta}{d\xi}$ in equation (5) gives,

$$\frac{d\Theta}{d\xi}=\frac{2}{3}\left(\gamma\text{-}1\right)M_0^2\left[\frac{\xi^5}{\left(1+\xi^4\right)^2}\right]+\frac{C_1}{\left(\xi+\xi^5\right)}$$

Inserting the boundary condition in above equation that requires the $\frac{d\Theta}{d\xi}$=0 at vortex center gives C_1=0 and equation reduces to,

$$\frac{d\Theta}{d\xi}=\frac{2}{3}(\gamma-1)M_0^2\left[\frac{\xi^5}{(1+\xi^4)^2}\right]$$

Integrating above equation once more yields,

$$\Theta=\frac{1}{6}(\gamma-1)M_0^2\left[\tan^{-}(\xi^2)-\left(\frac{\xi^2}{1+\xi^4}\right)\right]+C_2 \tag{6}$$

C_2 is constant of integration determined by applying second boundary condition that requires the temperature attain its ambient value $(\Theta\to 1)$ as $\xi\to\infty$,

$$C_2=1-\frac{1}{6}(\gamma-1)M_0^2\left(\frac{\pi}{2}\right)$$

Inserting C_2 in equation (6) gives the radial distribution of temperature,

$$\Theta=1+\frac{1}{6}(\gamma-1)M_0^2\left[\tan^{-}(\xi^2)-\frac{\xi^2}{1+\xi^4}-\frac{\pi}{2}\right]$$

This is the exact solution of energy equation under laminar compressible vortex flow conditions valid for a Pr=2/3.

(ii) Entropy Equation

Oswatitsch's entropy (1945) equation is given by,

$$\Theta PrU\frac{d(\Delta S)}{d\xi}=\frac{1}{\xi}\frac{d}{d\xi}\left(\xi\frac{d\Theta}{d\xi}\right)+Pr(\gamma-1)M_0^2 f \tag{1}$$

Subjected to boundary condition $\Delta S\to 0$ as $\xi\to\infty$, where $\Delta S=\frac{s-s_\infty}{c_p}$

The value of L.H.S. of equation (1) is determined by rearranging the terms of equation (3.1.12) yields,

$$\frac{1}{\xi}\frac{d}{d\xi}\left[\xi\frac{d\Theta}{d\xi}\right]+\Pr\left(\gamma-1\right)M_0^2 f=\Pr U\frac{d\Theta}{d\xi}-\Pr\left(\gamma-1\right)M_0^2\frac{UV^2}{\xi} \tag{2}$$

Comparing equations (1) and (2) gives following expression of entropy,

$$\Theta\Pr U\frac{d\left(\Delta S\right)}{d\xi}=\Pr U\frac{d\Theta}{d\xi}-\Pr\left(\gamma-1\right)M_0^2\frac{UV^2}{\xi}$$

or

$$d\left(\Delta S\right)=\frac{1}{\Theta}d\Theta-\left(\gamma-1\right)M_0^2\frac{V^2}{\xi\Theta}d\xi$$

Integrating above equation from 0 to ξ produces

$$\int_0^{\xi}d\left(\Delta S\right)=\int_0^{\xi}\frac{1}{\Theta}d\Theta-\left(\gamma-1\right)M_0^2\int_0^{\xi}\frac{V^2}{\xi\Theta}d\xi$$

$$\left(\Delta S\right)_{\xi}-\left(\Delta S\right)_{\xi=0}=\left[\ln(\Theta)_{\xi}-\ln(\Theta)_{\xi=0}\right]-\left(\gamma-1\right)M_0^2\int_0^{\xi}\frac{V^2}{\xi\Theta}d\xi+C_1 \tag{3}$$

C_1 is the constant of integration and is calculated using boundary condition at far away from vortex center that requires,

As $\xi\to\infty$, $\Delta S\to 0$ and $\Theta\to 1$, gives

$$C_1=\ln(\Theta)_{\xi=0}+\left(\gamma-1\right)M_0^2\int_0^{\infty}\frac{V^2}{\xi\Theta}d\xi-\left(\Delta S\right)_{\xi=0}$$

Inserting value of C_1 in equation (3) gives the radial distribution of change in entropy,

$$\left(\Delta S\right)_{\xi} = \ln(\Theta)_{\xi} + \left(\gamma - 1\right) M_0^2 \left[\int_0^{\infty} \frac{V^2}{\xi\Theta} d\xi - \int_0^{\xi} \frac{V^2}{\xi\Theta} d\xi \right] \tag{4}$$

This is the entropy equation valid for both laminar and turbulent compressible vortex flow.

Appendix B

(i) Source Code for Laminar Compressible Vortex Flow

```
function[Chi,Theta,Texactsolution,Beta,Pi,DeltaS,F,D,h]=LaminarFlow(M0,Pr,xf,N)

% N represents number of parts
% h represents the step size
% i represents the number of nodes
% Pr is Parandtl number
% gamma is specific heat ratio
% xf is the value of dimensionless radius at infinity
% M0 is vortex Mach number
% F represents heating of fluid element due to friction
% D represents cooling of fluid element due to its expansion
% lambda represents integration factor
% DT represents derivative of Temperature w.r.t. to x
% Tzero Represents value of temperature at vortex center

% U = ((-6.*(x.^3))./(1+x.^4))
% f = ((4.*(x.^8))./((1+x.^4).^3))
% V = (x./((1+x.^4).^(0.5)))
% Vsquare = ((x.^2)./(1+x.^4))
% F1 = (f.*x + U.*(V.^2))*lambda
% F2  =x*lambda
% F3 = Vsquare/x
% F4 = Vsquare/x
% F5 = f*x*Lambda
% F6 = U*Vsquare*Lambda

format long
gamma = 1.4;
h =(xf)/N;
i =N+1;

for i=1:(N+1)
x(i) = (i-0.5)*h ;%Integral is calculated at center of each node
end

lambda  = ((1+(x.^4)).*((6.*Pr)./4));
for n =1:N
F1 = @ (x) ((((4.*(x.^9))./((1+x.^4).^3))+((-
6.*(x.^3))./(1+x.^4)).*((x.^2)./(1+x.^4))).*((1+(x.^4)).*((6.*Pr)./4))) ;
UpperIntegral(n) = quadl(F1,0,x(n));
```

```
end

for o =1:N
F2(o)  = x(o)*lambda(o);
Height(o) = UpperIntegral(o)/F2(o) ;
base  = h;
Strip = Height.*(h); % Represents area of small strip
SummationofStrips  = sum(Strip);
Tzero = 1+ Pr*(gamma-1)*(M0^2)*SummationofStrips;
end

addition (1)=Strip(1);

for p= 2:N
addition(p)  = addition(p-1)+Strip(p);
end

for q =1:N
T(q) = -Pr*(gamma-1)*M0^2*addition(q)+Tzero;
end

Chi = 0:h:xf ;
Theta = [Tzero T];
Texactsolution = 1+ ((gamma-1).*(M0.^2)./6).*(atan(Chi.^2) - ((Chi.^2)./(1+Chi.^4))-
pi./2) ;
```

%% Calculations of Density and Pressure

```
for r=1:N+1
F3 = @ (Chi) ((Chi)./(1+(Chi.^4)))  ;
DensityIntegralConstant = quadl(F3,0,xf);
DensityIntegral(r) = quadl(F3,0,Chi(r));
Beta(r)              =              (1/(Theta(r)))*exp(gamma*(M0^2)*(DensityIntegral(r)-
DensityIntegralConstant)/Theta(r)) ;
Pi(r) = Beta(r)*Theta(r) ;
end
```

%% Calculation of Entropy

```
for s=1:N+1
F4 = @ (Chi) (Chi./(1+Chi.^4))  ;
EntropyIntegralConstant = quadl(F4,0,xf);
EntropyIntegral(s) = quadl(F4,0,Chi(s));
DeltaS(s)   =   log(Theta(s))+((gamma-1)*(M0^2)/Theta(s))*(EntropyIntegralConstant-
EntropyIntegral(s));
end
```

```
x1= Chi(2:N+1);
Lambda = ((1+(x1.^4)).*((6.*Pr)./4))  ;
LowerValue = x1.*Lambda ;
```

%% Calculation of heating (F) due to Viscous Dissipation and Cooling (D) of fluid element due to its expansion

```
for t =1:N
F5 = @ (x1) (((4.*(x1.^9))./((1+x1.^4).^3)).*((1+(x1.^4)).*((6.*Pr)./4)));
F6 = @ (x1) (((-
6.*(x1.^3))./(1+x1.^4)).*((x1.^2)./(1+x1.^4)).*((1+(x1.^4)).*((6.*Pr)./4)));
upperF(t) = quadl(F5,0,x1(t));
upperD(t) = quadl(F6,0,x1(t));
end

hdtf = Pr.*(gamma-1).*(M0.^2).*upperF./LowerValue;
cdte = Pr.*(gamma-1).*(M0.^2).*upperD./LowerValue;
F = [0 hdtf];
D = [0 cdte];
DT = F+D;
end
```

(ii) Source Code for Turbulent Compressible Vortex Flow

```
function[Chi,Theta,Thetamax,Chim,Beta,Pi,DeltaS,F,D,h]=TurbulentFlow(M0,Pr,xf,N,a)

% N represents number of parts
% h represents the step size
% i represents the number of nodes
% a is Scaling Constant represents degree Turbulence
% Pr is Parandtl number
% gamma is specific heat ratio
% xf is the value of dimensionless radius at infinity
% M0 is vortex Mach number
% F represents heating of fluid element due to friction
% D represents cooling of fluid element due to its expansion
% lambda represents integration factor
% Tzero represents the value of temperature at vortex center
% Chim is the Location of x corresponds to Thetamax


% f = ((16.*(m.^2).*((a+1).^(2.*m)).*(x.^8))./((a+(x.^4)).^(2.*(m+1))))
% V       = ((((a+1).^m).*x)./((a+(x.^4)).^m))
```

```
% Vsquare = ((x.^2).*(((a+1)./(a+(x.^4))).^(2.*m)))
% F1      = (f.*x + U.*(V.^2))*lambda
% F2      = x*lambda
% F3      = Vsquare/x
% F4      = Vsquare/x
% F5      = f*x*Lambda
% F6      = U*Vsquare*Lambda

format long
gamma=1.4;
h =(xf)/N;
i =N+1;

for i=1:(N+1)    % Integral is calculated at center of each node
x(i) = (i-0.5)*h ;
end

m     = (a+1)/4;
b1    = -((2*m)-1); % m,b1,b2,b3 are constants
b2    = -2*a*(m-1) ;
b3    = (a)^2;
U                                                    =                                                    (-
((4.*m.*b1.*(x.^7)./(b1.*(x.^8)+b2.*(x.^4)+b3))+(12.*a.*m.*(x.^3)./(b1.*(x.^8)+b2.*(x.
^4)+b3))));
lambda   =   ((((2.*b1.*(x.^4)+   b2-((((b2).^2)-   4.*b1.*b3).^(0.5))).(2.*b1.*(x.^4)+   b2
+((((b2).^2)-                  4.*b1.*b3).^(0.5)))).^(                  3.*a.*m.*Pr./((((b2).^2)-
4.*b1.*b3).^(0.5)))).*((((b1.*(x.^8)   +   b2.*(x.^4)+b3).^(1./(2.*b1))).(((2.*b1.*(x.^4)+
b2-((((b2).^2)-          4.*b1.*b3).^(0.5))).(2.*b1.*(x.^4)+          b2          +((((b2).^2)-
4.*b1.*b3).^(0.5)))).^( b2./(((((b2).^2)- 4.*b1.*b3).^(0.5)).*2.*b1)))).^(m.*b1.*Pr)));

for n =1:N
F1  =  @  (x)  ((((16.*(m.^2).*((a+1).^(2.*m)).*(x.^9)).(((a+(x.^4)).^(2.*(m+1))))+((-
((4.*m.*b1.*(x.^7)./(b1.*(x.^8)+b2.*(x.^4)+b3))+(12.*a.*m.*(x.^3)./(b1.*(x.^8)+b2.*(x.
^4)+b3)))).*((x.^2).*(((a+1).(a+(x.^4))).^(2.*m))))).*((((2.*b1.*(x.^4)+   b2-((((b2).^2)-
4.*b1.*b3).^(0.5))).(2.*b1.*(x.^4)+       b2       +((((b2).^2)-       4.*b1.*b3).^(0.5)))).^(
3.*a.*m.*Pr./((((b2).^2)-                  4.*b1.*b3).^(0.5)))).*((((b1.*(x.^8)                  +
b2.*(x.^4)+b3).^(1./(2.*b1))).(((2.*b1.*(x.^4)+                                b2-((((b2).^2)-
4.*b1.*b3).^(0.5))).(2.*b1.*(x.^4)+       b2       +((((b2).^2)-       4.*b1.*b3).^(0.5)))).^(
b2./(((((b2).^2)- 4.*b1.*b3).^(0.5)).*2.*b1)))).^(m.*b1.*Pr))));
UpperIntegral(n) = quadl(F1,0,x(n));
end

for o =1:N
F2(o)  = x(o)*lambda(o);
Height(o) = UpperIntegral(o)/F2(o) ;
base  = h;
```

```
Strip = Height.*(h); % Represents area of small strip
SummationofStrips  = sum(Strip);
Tzero = 1+ Pr*(gamma-1)*(M0^2)*SummationofStrips;
end

addition(1)=Strip(1);
for p= 2:N
addition(p)  = addition(p-1)+Strip(p);
end

for q =1:N
T(q) = -Pr*(gamma-1)*M0^2*addition(q)+Tzero;
end

Chi = 0:h:xf ;
Theta = [Tzero T];
Thetamax = max(Theta) ;
Chim = Chi(Theta == Thetamax);
```

%% Calculations of Density and Pressure

```
for r=1:N+1
F3 = @ (Chi) (Chi.*(((a+1)./(a+(Chi.^4))).^(2.*m)))  ;
DensityIntegralConstant = quadl(F3,0,xf);
DensityIntegral(r) = quadl(F3,0,Chi(r));
Beta(r) = (1/(Theta(r)))*exp(gamma*(M0^2)*(DensityIntegral(r)-
DensityIntegralConstant)/Theta(r)) ;
Pi(r) =  Beta(r)*Theta(r) ;
end
```

%% Entropy calculation

```
for s=1:N+1
F4 = @ (Chi) (Chi.*(((a+1)./(a+(Chi.^4))).^(2.*m)))  ;
EntropyIntegralConstant = quadl(F4,0,xf);
EntropyIntegral(s) = quadl(F4,0,Chi(s));
DeltaS(s) = log(Theta(s))+((gamma-1)*(M0^2)/Theta(s))*(EntropyIntegralConstant-
EntropyIntegral(s));
end

x1= Chi(2:N+1);
Lambda  = ((((2.*b1.*(x1.^4)+ b2-((((b2).^2)- 4.*b1.*b3).^(0.5))./(2.*b1.*(x1.^4)+ b2
+((((b2).^2)- 4.*b1.*b3).^(0.5)))).^( 3.*a.*m.*Pr./((((b2).^2)-
4.*b1.*b3).^(0.5)))).*((((b1.*(x1.^8) + b2.*(x1.^4)+b3).^(1./(2.*b1))./(((2.*b1.*(x1.^4)+
b2-((((b2).^2)- 4.*b1.*b3).^(0.5))./(2.*b1.*(x1.^4)+ b2 +((((b2).^2)-
4.*b1.*b3).^(0.5)))).^( b2./(((((b2).^2)- 4.*b1.*b3).^(0.5)).*2.*b1)))).^(m.*b1.*Pr))) ;
```

```
LowerValue = x1.*Lambda ;
```

%% Calculation of heating (F) due to Viscous Dissipation and Cooling (D) of fluid element due to its expansion

```
for t =1:N
F5 = @ (x1) (((16.*(m.^2).*((a+1).^(2.*m)).*(x1.^9))./((a+(x1.^4)).^(2.*(m+1)))).*((((2.*b1.*(x1.^4) + b2-((((b2).^2)- 4.*b1.*b3).^(0.5)))./(2.*b1.*(x1.^4)+ b2 +((((b2).^2)- 4.*b1.*b3).^(0.5)))).^( 3.*a.*m.*Pr./((((b2).^2)- 4.*b1.*b3).^(0.5)))).*((((b1.*(x1.^8) + b2.*(x1.^4)+b3).^(1./(2.*b1))).*(((2.*b1.*(x1.^4)+ b2-((((b2).^2)- 4.*b1.*b3).^(0.5)))./(2.*b1.*(x1.^4)+ b2 +((((b2).^2)- 4.*b1.*b3).^(0.5)))).^( b2./(((((b2).^2)- 4.*b1.*b3).^(0.5)).*2.*b1)))).^(m.*b1.*Pr))));

F6 = @ (x1) ((-((4.*m.*b1.*(x1.^7)./(b1.*(x1.^8)+b2.*(x1.^4)+b3))+(12.*a.*m.*(x1.^3)./(b1.*(x1.^8)+b2.*(x1.^4)+b3)))).*((x1.^2).*(((a+1)./(a+(x1.^4))).^(2.*m))).*((((2.*b1.*(x1.^4)+ b2-((((b2).^2)- 4.*b1.*b3).^(0.5)))./(2.*b1.*(x1.^4)+ b2 +((((b2).^2)- 4.*b1.*b3).^(0.5)))).^( 3.*a.*m.*Pr./((((b2).^2)- 4.*b1.*b3).^(0.5)))).*((((b1.*(x1.^8) + b2.*(x1.^4)+b3).^(1./(2.*b1))).*(((2.*b1.*(x1.^4)+ b2-((((b2).^2)- 4.*b1.*b3).^(0.5)))./(2.*b1.*(x1.^4)+ b2 +((((b2).^2)- 4.*b1.*b3).^(0.5)))).^( b2./(((((b2).^2)- 4.*b1.*b3).^(0.5)).*2.*b1)))).^(m.*b1.*Pr))));

upperF(t) = quadl(F5,0,x1(t));
upperD(t) = quadl(F6,0,x1(t));
end

hdtf = Pr.*(gamma-1).*(M0.^2).*upperF./LowerValue;
cdte = Pr.*(gamma-1).*(M0.^2).*upperD./LowerValue;
F = [0 hdtf];
D = [0 cdte];
DT = F+D;
end
```